

SCET sum rules for $\Lambda_b \rightarrow \Lambda \ell^+ \ell^-$, $\Lambda \gamma$ decays

Long-Shun Lu^{a,b1}, Cai-Dian Lü^{a,b}, Yue-Long Shen^c, Yan-Bing Wei^d

^a *Institute of High Energy Physics, CAS, P.O. Box 918(4) Beijing 100049, China*

^b *School of Physics, University of Chinese Academy of Sciences, Beijing 100049, China*

^c *College of Information Science and Engineering, Ocean University of China, Songling Road 238, Qingdao, 266100 Shandong, P.R. China*

^d *Institute of Particle Physics and Key Laboratory of Quark and Lepton Physics (MOE), Central China Normal University, Wuhan, Hubei 430079, China*

Abstract

We construct light-cone sum rules for various types of effective form factors in the $\Lambda_b \rightarrow \Lambda \ell^+ \ell^-$ and $\Lambda_b \rightarrow \Lambda \gamma$ decays by analyzing vacuum-to- Λ_b (or γ^* -to- Λ_b) correlation functions with the light Λ -baryon interpolating current. These form factors, defined via hadronic matrix elements within soft-collinear effective theory (SCET), enter the next-to-leading-power QCD factorization formulas for large-recoil transitions. Implementing the perturbative matching from SCET_I to heavy quark effective theory, we determine the hard-collinear functions at next-to-leading-order accuracy. Based on light-cone sum rule predictions for the $\Lambda_b \rightarrow \Lambda$ form factors, we compute the q^2 -dependent differential branching fraction, forward-backward asymmetry and dilepton longitudinal polarization fraction for $\Lambda_b \rightarrow \Lambda \ell^+ \ell^-$ decay, as well as the branching fraction for $\Lambda_b \rightarrow \Lambda \gamma$ decay.

arXiv:2506.21419v2 [hep-ph] 1 Jul 2025

¹E-mail: lulongshun@ihep.ac.cn

Contents

1	Introduction	1
2	SCET analysis for $\Lambda_b \rightarrow \Lambda \ell^+ \ell^-$, $\Lambda \gamma$ decays	3
2.1	The operators in SCET	4
2.2	The decay amplitudes in SCET	6
3	LCSR for the SCET form factors	8
3.1	LCSR for A-type soft form factor	10
3.1.1	Correlation function at tree level	10
3.1.2	Factorization of the correlation function at $\mathcal{O}(\alpha_s)$	11
3.1.3	Leading power contribution	12
3.1.4	Factorization-scale independence	13
3.1.5	LCSR of $\xi_\Lambda(n \cdot p)$ at $\mathcal{O}(\alpha_s)$	14
3.2	LCSR for B-type form factor	15
3.3	LCSR for C-type non-factorisable contributions	16
4	Numerical results	19
4.1	Input parameters	19
4.2	Predictions for the $\Lambda_b \rightarrow \Lambda$ effective form factors	22
5	Phenomenological applications	25
6	Conclusions	27
A	Light-Cone Distribution Amplitudes	28
B	Decay distribution in the helicity formalism	31

1 Introduction

It is widely recognized that decays of bottom hadrons induced by the flavor-changing neutral current (FCNC) transition $b \rightarrow s \ell^+ \ell^-$, with $\ell = e, \mu, \tau$, serve as sensitive probes of physics beyond the Standard Model (SM) [1, 2]. Thanks to the large datasets collected at the Large Hadron Collider (LHC) and the Super B Factory, the properties of many exclusive $b \rightarrow s \ell^+ \ell^-$ decay channels have been measured with unprecedented precision. The accumulation of additional data is expected to further enhance the statistical power of these measurements in the near future. The measured observables in $b \rightarrow s \ell^+ \ell^-$ decay providing valuable inputs for testing theoretical predictions and refining our understanding of rare bottom-hadron decays. Notably, tensions still exist between SM predictions and experimental measurements of these observables, particularly in the differential branching fractions and angular observables in the large-recoil region. Transition form factors, such as those in $B \rightarrow K^*$ and $B_s \rightarrow \phi$ decays, are essential nonperturbative inputs in exclusive $b \rightarrow s \ell^+ \ell^-$ processes. These form factors have been carefully calculated using lattice QCD in the low-recoil region [3, 4]. In the large-recoil region, their predictions rely on extrapolation models, which can be improved by combining direct calculations with light-cone sum rules (LCSR) [5, 6]. Non-local hadronic matrix elements can also significantly affect the observables, and are more challenging on the theoretical side. Although considerable effort has been devoted to evaluating such matrix elements, they continue to be a major source of theoretical uncertainty.

The baryon decay modes $\Lambda_b \rightarrow \Lambda \ell^+ \ell^-$ offer new insights into the existing tensions between

SM predictions and experimental data [7]. These decays also provide a rich set of angular observables that can help disentangle the contributions from different operators in the weak effective Hamiltonian. The decay $\Lambda_b \rightarrow \Lambda(\rightarrow p\pi)\ell^+\ell^-$ involves three angular variables, even when both the Λ_b baryon and the proton are unpolarized [8,9]. Moreover, since the Λ is a ground-state baryon, the $\Lambda_b \rightarrow \Lambda$ transition form factors can be predicted with relatively higher accuracy, compared to those for $B \rightarrow K^*$ transitions. Similarly, the radiative decay $\Lambda_b \rightarrow \Lambda\gamma$ serves as a sensitive probe of the $b \rightarrow s\gamma$ transition, where the SM predicts predominantly left-handed photon polarization [10]. The helicity of the final-state Λ baryon is experimentally accessible, providing direct information about the photon polarization structure and enabling complementary constraints on possible right-handed currents beyond those observed in B -meson decays. Taken together, these Λ_b decay channels serve as golden modes for precision tests of the SM and for probing potential new physics scenarios.

The decay amplitudes of the $\Lambda_b \rightarrow \Lambda\ell^+\ell^-$, $\Lambda\gamma$ processes are determined by the matrix elements $\langle \ell^+\ell^-(\gamma)\Lambda | \mathcal{O}_i | \Lambda_b \rangle$, where \mathcal{O}_i are the effective operators in the weak Hamiltonian. The most important hadronic inputs are the $\Lambda_b \rightarrow \Lambda$ transition form factors, which arise from the matrix elements of the semileptonic or electromagnetic operators. The $\Lambda_b \rightarrow \Lambda$ form factors in the small recoil region can be obtained from lattice-QCD studies [11,12], and in the large recoil region one could employ LCSR to obtain relatively reliable predictions [13–15]. In the heavy b -quark limit, the number of independent form factors is reduced from ten to two at small recoil, and large recoil symmetry further reduces this number to one [14,16]. In the context of soft-collinear effective theory (SCET) [17–19], this large recoil symmetry can be described in a more transparent and systematic way, allowing for an expansion of the form factors in powers of Λ_{QCD}/m_b [20]. It has been established that the leading-power contribution originates from hard-collinear gluon exchange diagrams, which however is numerically subdominant compared to the soft contribution [14]. Beyond the local form factor contributions, the matrix elements of four-quark operators and the chromo-magnetic operator give rise to so-called “nonlocal form factors.” These include effects such as long-distance quark-loop contributions and the “annihilation topology contribution,” among others. In [21], the leading annihilation topology contribution was studied, revealing that it induces corrections of approximately 1% relative to the local form factor contribution.

In this article, we perform a systematic analysis of the $\Lambda_b \rightarrow \Lambda\ell^+\ell^-$ and $\Lambda_b \rightarrow \Lambda\gamma$ decays within the framework of SCET. Starting from the effective Hamiltonian for weak interactions in heavy quark decays, we match the effective operators onto the SCET_I operators. Since this work considers amplitudes only up to $\mathcal{O}(\alpha_s)$, we do not include SCET_I operators involving more than one gluon field. The relevant SCET_I operators can be categorized into three types: A-type, B-type, and C-type. The decay amplitudes are then expressed as the product and convolution of effective hard functions and the matrix elements of SCET_I operators. We employ LCSR to evaluate the matrix elements of the A-type, B-type, and C-type operators, respectively. Among these, the A-type operators yield the dominant contributions. Since the leading-power amplitude starts at $\mathcal{O}(\alpha_s^2)$, our analysis primarily focuses on the soft form factors that preserve large recoil symmetry. At the amplitude level, we find that the B-type operator contributions are strongly suppressed and can be neglected, while the non-

factorizable C-type contributions are numerically insignificant. Consequently, the Λ_b decay processes are dominated by soft contributions.

The remainder of this article is organized as follows. In the next section, we conduct a theoretical analysis of the $\Lambda_b \rightarrow \Lambda \ell^+ \ell^-$ and $\Lambda_b \rightarrow \Lambda \gamma$ decay amplitudes within the framework of SCET. In Section 3, we construct light-cone sum rules for the SCET $\Lambda_b \rightarrow \Lambda$ form factors, utilizing the distribution amplitude of the Λ_b baryon. Numerical results are presented in Section 4. Section 5 discusses several phenomenological applications. The final section concludes the article with a summary.

2 SCET analysis for $\Lambda_b \rightarrow \Lambda \ell^+ \ell^-$, $\Lambda \gamma$ decays

In this section, we perform an analysis of the $\Lambda_b \rightarrow \Lambda \ell^+ \ell^-$ and $\Lambda_b \rightarrow \Lambda \gamma$ decays within the framework of SCET. In the rest frame of the Λ_b baryon, the final-state Λ baryon moves at high velocity, and we assume that the momenta of the quarks inside the Λ baryon are aligned along a light-cone direction \bar{n} . For the $\Lambda_b \rightarrow \Lambda \gamma$ decay, the momentum of the photon is given by $q_\gamma = E_\gamma \bar{n}$, with $\bar{n} \cdot n = 2$. For the $\Lambda_b \rightarrow \Lambda \ell^+ \ell^-$ decays, we restrict our analysis to the kinematic region $1 \text{ GeV}^2 < q^2 < 7 \text{ GeV}^2$, where q denotes the momentum of the lepton pair. In this region, resonance effects can be safely neglected.

A given momentum p can be decomposed as $p^\mu = n \cdot p \bar{n}^\mu / 2 + \bar{n} \cdot p n^\mu / 2 + p_\perp^\mu$. The momentum of the Λ baryon follows the power-counting rule

$$p = (n \cdot p, \bar{n} \cdot p, p_\perp) \sim (1, \lambda^4, \lambda^2) m_b, \quad (1)$$

with $\lambda \sim \sqrt{\Lambda_{\text{QCD}}/m_b}$. In addition to this collinear momentum mode, the power counting for the soft and hard-collinear modes is $(\lambda^2, \lambda^2, \lambda^2) m_b$ and $(1, \lambda^2, \lambda) m_b$, respectively. Moreover, the anti-collinear photon and the anti-hard-collinear lepton pair scale as $q_\gamma \sim (\lambda^4, 1, \lambda^2) m_b$ and $q \sim (\lambda^2, 1, \lambda) m_b$, respectively. The fields in SCET, in terms of gauge invariant building blocks [22], also have definite power counting

$$\xi_q \sim \lambda, \quad \chi_q \sim \lambda, \quad A_{hc}^\mu \sim (1, \lambda^2, \lambda), \quad A_{hc\perp}^{(\text{em})} \sim \lambda, \quad q_q \sim \lambda^3, \quad h \sim \lambda^3. \quad (2)$$

Above, the symbols ξ_q , χ_q , q_q and h stand for the hard-collinear, anti-hard-collinear, soft quark and effective heavy quark fields, respectively, where the subscript $q = u, d, s$ denotes the flavor of the light quarks. The symbols A_{hc}^μ and $A_{hc\perp}^{(\text{em})}$ stand for hard-collinear gluon field and anti-hard-collinear photon field, separately.

Since there exist both hard-collinear and collinear fields, two effective theories are introduced. The first is an intermediate effective theory, denoted as SCET_I, which contains soft and hard-collinear degrees of freedom. The second is the final infrared theory, referred to as SCET_{II}, which contains soft and collinear fields. For a factorizable process, long-distance nonperturbative quantities, such as the light-cone distribution amplitudes (LCDAs) of the initial- and final-state hadrons, are described by the matrix elements of SCET_{II} operators. The perturbative functions can be computed through a two-step matching procedure: QCD \rightarrow SCET_I \rightarrow SCET_{II}.

2.1 The operators in SCET

The effective weak Hamiltonian for the semileptonic $b \rightarrow s\ell^+\ell^-$, $s\gamma$ transitions in the SM can be written as [23]

$$\mathcal{H}_{\text{eff}} = -\frac{G_F}{\sqrt{2}} \left[V_{tb}V_{ts}^* \mathcal{H}_{\text{eff}}^{(t)} + V_{ub}V_{us}^* \mathcal{H}_{\text{eff}}^{(u)} \right] + \text{h.c.}, \quad (3)$$

where we have employed the unitarity relations of the Cabibbo-Kobayashi-Maskawa (CKM) matrix elements, and

$$\begin{aligned} \mathcal{H}_{\text{eff}}^{(t)} &= C_1 \mathcal{Q}_1^c + C_2 \mathcal{Q}_2^c + \sum_{i=3,\dots,10} C_i \mathcal{Q}_i, \\ \mathcal{H}_{\text{eff}}^{(u)} &= C_1 (\mathcal{Q}_1^c - \mathcal{Q}_1^u) + C_2 (\mathcal{Q}_2^c - \mathcal{Q}_2^u). \end{aligned} \quad (4)$$

Since $\mathcal{H}_{\text{eff}}^{(u)}$ is doubly Cabibbo-suppressed, it can be safely neglected. In full QCD, the hadronic matrix elements of the semileptonic operators $\mathcal{Q}_{7,9,10}$ can be readily expressed in terms of the heavy-to-light $\Lambda_b \rightarrow \Lambda$ decay form factors [14, 15]. The remaining contributions to the electroweak penguin decay amplitude can be determined by contracting the exclusive $\Lambda_b \rightarrow \Lambda\gamma^*$ matrix element with the vector lepton current $\gamma^* \rightarrow \ell^+\ell^-$ in the $\Lambda_b \rightarrow \Lambda\ell^+\ell^-$ decay.

The matching from QCD to SCET_I can be expressed as

$$\begin{aligned} \mathcal{H}_{b \rightarrow s\ell^+\ell^-} &= \sum_{i=1}^4 \int ds \tilde{C}_i^A(s) Q_i^A(s) + \sum_{j=1}^4 \int ds \int dr \tilde{C}_j^B(s, r) Q_j^B(s, r) \\ &+ \sum_{k=1}^4 \int ds \int dr \int dt \tilde{C}_k^C(s, r, t) Q_k^C(s, r, t) + \dots, \end{aligned} \quad (5)$$

$$\begin{aligned} \mathcal{H}_{b \rightarrow s\gamma} &= \int ds \int dt \tilde{C}_\gamma^A(s, t) Q_\gamma^A(s, t) + \sum_{j=1}^2 \int ds \int dr \int dt \tilde{C}_{\gamma,j}^B(s, r, t) Q_{\gamma,j}^B(s, r, t) \\ &+ \sum_{k=1}^4 \int ds \int dr \int dt \tilde{C}_k^C(s, r, t) Q_k^C(s, r, t) + \dots, \end{aligned} \quad (6)$$

where $\tilde{C}_i^{(A,B,C)}$, \tilde{C}_γ^A , and $\tilde{C}_{\gamma,i}^B$ are hard functions in position space. These are related to the momentum-space hard functions via the Fourier transformations:

$$\begin{aligned} C_i^A(n \cdot p) &= \int ds e^{isn \cdot p} \tilde{C}_i^A(s), \\ C_i^B(n \cdot p, u) &= \int ds \int dr e^{i(us + \bar{u}r)n \cdot p} \tilde{C}_i^B(s, r), \\ C_\gamma^A(n \cdot p) &= \int ds \int dt e^{isn \cdot p} e^{it\bar{n} \cdot q} \tilde{C}_\gamma^A(s, t), \\ C_{\gamma,i}^B(n \cdot p, u) &= \int ds \int dr \int dt e^{i(us + \bar{u}r)n \cdot p} e^{it\bar{n} \cdot q} \tilde{C}_{\gamma,i}^B(s, r, t), \\ C_i^C(n \cdot p, u) &= \int ds \int dr \int dt e^{i(us + \bar{u}r)n \cdot p} e^{it\bar{n} \cdot q} \tilde{C}_i^C(s, r, t), \end{aligned} \quad (7)$$

with $\bar{u} = 1 - u$.

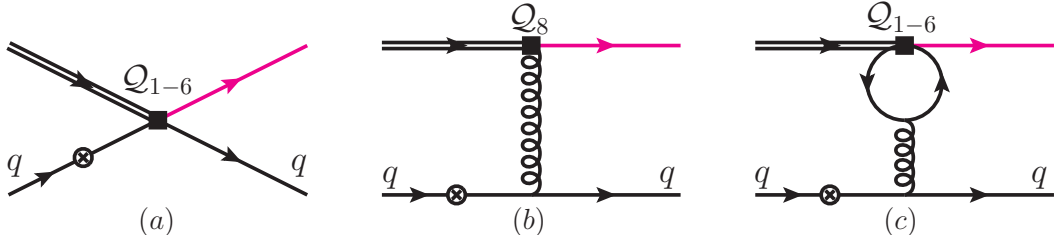


Figure 1: Feynman diagrams where the (virtual) photon, as denoted by the crossed circle, is emitted from the spectator light quark q . The b -quark is indicated by a double line; the strange quark by a magenta line.

The A-type and B-type SCET_I operators for $b \rightarrow s \ell^+ \ell^-$ decay are given by [24]:

$$\begin{aligned}
Q_{1(3)}^A &= \bar{\xi}_s(sn)(1 + \gamma_5)\gamma_\perp^\mu h(0) \bar{\ell}\gamma_\mu(\gamma_\mu\gamma_5)\ell, \\
Q_{2(4)}^A &= \bar{\xi}_s(sn)(1 + \gamma_5)\frac{\bar{n}^\mu}{\bar{n} \cdot v}h(0) \bar{\ell}\gamma_\mu(\gamma_\mu\gamma_5)\ell, \\
Q_{1(3)}^B &= \bar{\xi}_s(sn)(1 + \gamma_5)\gamma_\perp^\mu \mathcal{A}_{hc\perp}(rn)h(0) \bar{\ell}\gamma_\mu(\gamma_\mu\gamma_5)\ell, \\
Q_{2(4)}^B &= \bar{\xi}_s(sn)(1 + \gamma_5)\mathcal{A}_{hc\perp}(rn)\frac{\bar{n}^\mu}{\bar{n} \cdot v}h(0) \bar{\ell}\gamma_\mu(\gamma_\mu\gamma_5)\ell,
\end{aligned} \tag{8}$$

and the operators for $b \rightarrow s\gamma$ decay are [25]:

$$\begin{aligned}
Q_\gamma^A &= \bar{\xi}_s(sn)(1 + \gamma_5)\mathcal{A}_{hc\perp}^{(\text{em})}(t\bar{n})h(0), \\
Q_{\gamma,1}^B &= \bar{\xi}_s(sn)(1 + \gamma_5)\mathcal{A}_{hc\perp}^{(\text{em})}(t\bar{n})\mathcal{A}_{hc\perp}(rn)h(0), \\
Q_{\gamma,2}^B &= \bar{\xi}_s(sn)(1 + \gamma_5)\mathcal{A}_{hc\perp}(rn)\mathcal{A}_{hc\perp}^{(\text{em})}(t\bar{n})h(0).
\end{aligned} \tag{9}$$

The A-type and B-type operators describe the emission of the (virtual) photon from the $b \rightarrow s$ transition currents, while the C-type operators Q_i^C correspond to diagrams in which the (virtual) photon is emitted from the spectator quark in the Λ_b baryon. These represent the non-factorizable contributions of the strong-penguin operators [21]. For both $\Lambda_b \rightarrow \Lambda \ell^+ \ell^-$ and $\Lambda_b \rightarrow \Lambda \gamma$ decays, the relevant C-type SCET_I operators are:

$$\begin{aligned}
Q_{1,3}^C &= \bar{\xi}_s(sn)(1 + \gamma_5)\gamma_\perp^\mu h(0) \bar{\xi}_q(rn)\gamma_\mu^\perp(1 \mp \gamma_5)\chi_q(t\bar{n}), \\
Q_{2,4}^C &= \bar{\xi}_s^i(sn)(1 + \gamma_5)\gamma_\perp^\mu h^j(0) \bar{\xi}_q^j(rn)\gamma_\mu^\perp(1 \mp \gamma_5)\chi_q^i(t\bar{n}),
\end{aligned} \tag{10}$$

where the subscript $q = u, d$ denotes the spectator quark that emits the (virtual) photon.

The hard functions of A-type operators have been calculated up to the two-loop level, except for the contributions from quark-loop diagrams with insertions of penguin operators. The coefficients of B-type operators are known at the one-loop level. In this work, we aim at a one-loop calculation of the decay amplitude. Therefore, we utilize the existing one-loop results for $C_i^{(A,B)}$ from [24], as well as C_γ^A and $C_{\gamma,i}^B$ from [25]. To obtain the hard functions of C-type operators, we consider the diagrams shown in Fig. 1, where the photon is emitted from the spectator quark. The calculation of the hard function up to α_s -level is analogous to the annihilation contribution to the $B \rightarrow \{\pi, K\} \ell^+ \ell^-$ decays [26]. We use the notation $\Delta_{16}^{(0)}C_i^C$, $\Delta_{12}^{(1)}C_i^C$ and $\Delta_8^{(1)}C_i^C$ stand for the matching of Q_{1-6} and Q_8 onto the C-type SCET_I operators C_i^C respectively. The annihilation-type leading topology is illustrated in diagram

(a) of Fig. 1, contributes to the matching coefficient C_i^C at order α_s^0 , for which the calculation is trivial:

$$\Delta_{16}^{(0)} C_{1,2,3,4}^C = -\frac{G_F}{\sqrt{2}} V_{tb} V_{ts}^* \bar{C}_{3,4,5,6}, \quad (11)$$

where the "barred" coefficients \bar{C}_{1-6} are related to the Wilson coefficients in the standard BBL basis [27] and the superscript (0) denotes the matching at order α_s^0 . The chromomagnetic contribution is originate from chromomagnetic operator \mathcal{Q}_8 at order α_s , as shown in diagram (b) of Fig. 1, matching onto the C-type SCET_I operators with the coefficients

$$\begin{aligned} \Delta_8^{(1)} C_1^C &= \Delta_8^{(1)} C_3^C = -\frac{G_F}{\sqrt{2}} V_{tb} V_{ts}^* \frac{1}{N_c} \frac{\alpha_s}{4\pi} \frac{C_8^{\text{eff}}}{1-u+u\hat{s}}, \\ \Delta_8^{(1)} C_2^C &= \Delta_8^{(1)} C_4^C = \frac{G_F}{\sqrt{2}} V_{tb} V_{ts}^* \frac{\alpha_s}{4\pi} \frac{C_8^{\text{eff}}}{1-u+u\hat{s}}, \end{aligned} \quad (12)$$

where $\hat{s} \equiv q^2/m_b^2$, $C_8^{\text{eff}} = C_8 + (4\bar{C}_3 - \bar{C}_5)/3$ [28]. Diagram (c) in Fig. 1 corresponds to the quark loops with spectator scattering (QLSS), which arise from the operators \mathcal{Q}_{1-6} at $\mathcal{O}(\alpha_s)$. The dominant contribution comes from the charm quark loop induced by \mathcal{Q}_2 due to its large Wilson coefficient. Since the penguin operators yield negligible effects, we omit their contributions. Thus, this diagram yields the following matching coefficients:

$$\begin{aligned} \Delta_{12}^{(1)} C_1^C &= \Delta_{12}^{(1)} C_3^C = \frac{G_F}{\sqrt{2}} V_{tb} V_{ts}^* \frac{1}{2N_c} \frac{\alpha_s}{4\pi} \bar{C}_2 G(u, \hat{s}, m_c^2/m_b^2), \\ \Delta_{12}^{(1)} C_2^C &= \Delta_{12}^{(1)} C_4^C = -N_c \Delta_{12}^{(1)} C_1^C = -N_c \Delta_{12}^{(1)} C_3^C, \end{aligned} \quad (13)$$

where the function $G(u, \hat{s}, \lambda)$ is defined as

$$G(u, \hat{s}, \lambda) = \frac{2}{3} + \frac{2}{3} \ln \frac{m_b^2}{\mu^2} + 4 \int_0^1 dx x(1-x) \ln [\lambda - x(1-x)(1-u+u\hat{s})]. \quad (14)$$

These subleading topologies from diagrams (b) and (c) in Fig. 1 are indeed numerically suppressed. Meanwhile, it is important to note that the contribution from diagram (c) of Fig. 1 is essential for eliminating the infrared divergence originating from the vertex correction diagrams in diagram (a) of Fig. 1. Finally, up to order α_s , we have:

$$C_i^C = \Delta_{16}^{(0)} C_i^C + \Delta_8^{(1)} C_i^C + \Delta_{12}^{(1)} C_i^C. \quad (15)$$

It is worth noting that we neglect the "vertex corrections" to the weak annihilation graph, and the matrix elements $\langle Q_i^C \rangle$ are computed only at tree level, given the the small Wilson coefficients of QCD penguin operators and the strong coupling constant. Consequently, the matching remains incomplete at order α_s .

2.2 The decay amplitudes in SCET

At the amplitude level, we consider standard relativistic normalization for hadronic states and have

$$\langle \Lambda(p, s') \ell^-(p_1, s_1) \ell^+(p_2, s_2) | -i \mathcal{H}_{b \rightarrow s \ell^+ \ell^-} | \Lambda_b(v, s) \rangle$$

$$= (2\pi)^4 \delta^4(M_{\Lambda_b} v - p - p_1 - p_2) i \mathcal{M}(s, s', s_1, s_2), \quad (16)$$

$$\langle \Lambda(p, s') \gamma(q, \lambda) | -i \mathcal{H}_{b \rightarrow s\gamma} | \Lambda_b(v, s) \rangle = (2\pi)^4 \delta^4(M_{\Lambda_b} v - p - q) i \mathcal{M}(s, s', \lambda), \quad (17)$$

where $\mathcal{M}(s, s', s_1, s_2)$ and $\mathcal{M}(s, s', \lambda)$ are the helicity amplitudes for the decays $\Lambda_b \rightarrow \Lambda \ell^+ \ell^-$ and $\Lambda_b \rightarrow \Lambda \gamma$, respectively. To obtain the factorized helicity amplitudes from Eq. (6), we must appropriately define form factors for the matrix elements of various SCET_I operators.

As noted in the introduction, within the heavy quark limit and large recoil limit, there exists a unique form factor $\xi_\Lambda(n \cdot p)$, which correspond to the matrix elements of A-type SCET_I operators [14, 16]

$$\langle \Lambda(p, s') | \bar{\xi}_s(0) \Gamma_i^A h(0) | \Lambda_b(v, s) \rangle = \xi_\Lambda(n \cdot p) \bar{u}_\Lambda(p, s') \Gamma_i^A u_{\Lambda_b}(v, s). \quad (18)$$

$\xi_\Lambda(n \cdot p)$ is assumed to be dominated by the soft gluon exchanges.

The matrix elements of B-type SCET_I operators correspond to hard-scattering corrections from hard-collinear gluon exchange [14], similar to the case of the $B \rightarrow P$ transition [29–31]. There is only one independent non-local form factor for B-type matrix elements, which we define as

$$\begin{aligned} & n \cdot p \int \frac{da}{2\pi} e^{-iun \cdot pa} \langle \Lambda(p, s') | \bar{\xi}_s(0) \Gamma_i^B A_{hc\perp}^\nu(an) h(0) | \Lambda_b(v, s) \rangle \\ &= M_{\Lambda_b} \Delta \xi_\Lambda^B(u, n \cdot p) \bar{u}_\Lambda(p, s') \gamma_\perp^\nu \Gamma_i^B u_{\Lambda_b}(v, s). \end{aligned} \quad (19)$$

The C-type contribution is referred to as a “non-factorisable contribution” [15, 21, 28, 32]. For the decay $\Lambda_b \rightarrow \Lambda \ell^+ \ell^-$, the lepton and hadronic parts can be factorized at the amplitude level:

$$\begin{aligned} & n \cdot p \int \frac{da}{2\pi} e^{-iun \cdot pa} \langle \Lambda(p, s') \ell^-(p_1, s_1) \ell^+(p_2, s_2) | Q_i^C(0, a, 0) | \Lambda_b(v, s) \rangle \\ &= g_{\text{em}} \frac{1}{q^2} \sum_\lambda \bar{\epsilon}^\mu(q, \lambda) \bar{u}(p_1, s_1) \gamma_\mu v(p_2, s_2) \\ & \quad \times n \cdot p \int \frac{da}{2\pi} e^{-iun \cdot pa} \langle \Lambda(p, s') \gamma^*(q, \lambda) | Q_i^C(0, a, 0) | \Lambda_b(v, s) \rangle, \end{aligned} \quad (20)$$

where $\bar{\epsilon}^\mu(q, \lambda)$ denotes the polarization vector of the virtual photon. The hadronic matrix elements of Q_i^C are parametrized in terms of form factors as follows:

$$\begin{aligned} & n \cdot p \int \frac{da}{2\pi} e^{-iun \cdot pa} \langle \Lambda(p, s') \gamma^*(q, \lambda) | Q_i^C(0, a, 0) | \Lambda_b(v, s) \rangle \\ &= g_{\text{em}} M_{\Lambda_b}^2 \bar{\epsilon}_\nu^*(q, \lambda) \Delta_i \xi_\Lambda^C(u, n \cdot p) \bar{u}_\Lambda(p, s') (1 + \gamma_5) \gamma_\perp^\nu u_{\Lambda_b}(v, s). \end{aligned} \quad (21)$$

In the decay $\Lambda_b \rightarrow \Lambda \gamma$ we have

$$\begin{aligned} & n \cdot p \int \frac{da}{2\pi} e^{-iun \cdot pa} \langle \Lambda(p, s') \gamma(q, \lambda) | Q_i^C(0, a, 0) | \Lambda_b(v, s) \rangle \\ &= g_{\text{em}} M_{\Lambda_b}^2 \epsilon_\nu^*(q, \lambda) \Delta_i \xi_\Lambda^C(u, n \cdot p) \bar{u}_\Lambda(p, s') (1 + \gamma_5) \gamma_\perp^\nu u_{\Lambda_b}(v, s), \end{aligned} \quad (22)$$

where $\epsilon_\nu^*(q, \lambda)$ denotes the polarization vector of the real photon.

Using the definitions of the SCET_I form factors, we can derive the factorized form of the helicity amplitudes. For the $\Lambda_b \rightarrow \Lambda \ell^+ \ell^-$ decay, we have

$$\begin{aligned}
\mathcal{M}(s, s', s_1, s_2) = & - \sum_{i=1}^4 \left\{ C_i^A(n \cdot p) \xi_\Lambda(n \cdot p) \bar{u}_\Lambda(p, s') \Gamma_i^A u_{\Lambda_b}(v, s) \bar{u}(p_1, s_1) \Gamma_i^{\ell\ell} v(p_2, s_2) \right. \\
& + M_{\Lambda_b} \int du C_i^B(n \cdot p, \bar{u}) \Delta \xi_\Lambda^B(u, n \cdot p) \bar{u}_\Lambda(p, s') \gamma_\perp^\nu \Gamma_i^B u_{\Lambda_b}(v, s) \bar{u}(p_1, s_1) \Gamma_i^{\ell\ell} v(p_2, s_2) \\
& - 16\pi^2 \frac{\alpha_e}{4\pi} \frac{1}{q^2} M_{\Lambda_b}^2 \int du C_i^C(n \cdot p, \bar{u}) \Delta_i \xi_\Lambda^C(u, n \cdot p) \bar{u}_\Lambda(p, s') (1 + \gamma_5) \gamma_\perp^\mu u_{\Lambda_b}(v, s) \\
& \left. \times \bar{u}(p_1, s_1) \gamma_\mu v(p_2, s_2) \right\}. \tag{23}
\end{aligned}$$

For the $\Lambda_b \rightarrow \Lambda \gamma$ decay, we have

$$\begin{aligned}
\mathcal{M}(s, s', \lambda) = & - \epsilon_\mu^*(q, \lambda) \left\{ C_\gamma^A(n \cdot p) \xi_\Lambda(q^2 = 0) \bar{u}_\Lambda(p, s') (1 + \gamma_5) \gamma_\perp^\mu u_{\Lambda_b}(v, s) \right. \\
& + M_{\Lambda_b} \sum_{j=1}^2 \int du C_{\gamma,j}^B(n \cdot p, \bar{u}) \Delta \xi_\Lambda^B(u, q^2 = 0) \bar{u}_\Lambda(p, s') \gamma_\perp^\nu \Gamma_{\gamma,j}^B u_{\Lambda_b}(v, s) \\
& \left. + g_{\text{em}} M_{\Lambda_b}^2 \sum_{k=1}^4 \int du C_k^C(n \cdot p, \bar{u}) \Delta_k \xi_\Lambda^C(u, q^2 = 0) \bar{u}_\Lambda(p, s') (1 + \gamma_5) \gamma_\perp^\mu u_{\Lambda_b}(v, s) \right\}. \tag{24}
\end{aligned}$$

The Dirac structures are defined as

$$\begin{aligned}
\Gamma_i^A = & \begin{cases} (1 + \gamma_5) \gamma_\perp^\mu & i = 1, 3 \\ (1 + \gamma_5) \frac{\bar{n}^\mu}{\bar{n} \cdot v} & i = 2, 4 \end{cases}, & \Gamma_i^{\ell\ell} = & \begin{cases} \gamma_\mu & i = 1, 2 \\ \gamma_\mu \gamma_5 & i = 3, 4 \end{cases}, \\
\Gamma_i^B = & \begin{cases} (1 + \gamma_5) \gamma_\perp^\mu \gamma_\nu & i = 1, 3 \\ (1 + \gamma_5) \frac{\bar{n}^\mu}{\bar{n} \cdot v} \gamma_\nu & i = 2, 4 \end{cases}, & \Gamma_{\gamma,j}^B = & \begin{cases} (1 + \gamma_5) \gamma_\perp^\mu \gamma_\nu & j = 1 \\ (1 + \gamma_5) \gamma_\nu \gamma_\perp^\mu & j = 2 \end{cases}.
\end{aligned} \tag{25}$$

As shown above, due to the identical spinor structures, the non-factorisable contributions to the $\Lambda_b \rightarrow \Lambda \ell^+ \ell^-$ and $\Lambda_b \rightarrow \Lambda \gamma$ decay amplitudes can be absorbed into the definitions of C_1^A and C_γ^A :

$$C_1^A \rightarrow C_1^A + \Delta C_1^A(q^2), \quad C_\gamma^A \rightarrow C_\gamma^A + \Delta C_\gamma^A(q^2 = 0), \tag{26}$$

where

$$\begin{aligned}
\Delta C_1^A(q^2) = & -16\pi^2 \frac{\alpha_e}{4\pi} \frac{1}{q^2} M_{\Lambda_b}^2 \sum_{i=1}^4 \int du C_i^C(n \cdot p, \bar{u}) \frac{\Delta_i \xi_\Lambda^C(u, n \cdot p)}{\xi_\Lambda(n \cdot p)}, \\
\Delta C_\gamma^A(q^2 = 0) = & g_{\text{em}} M_{\Lambda_b}^2 \sum_{i=1}^4 \int du C_i^C(n \cdot p, \bar{u}) \frac{\Delta_i \xi_\Lambda^C(u, q^2 = 0)}{\xi_\Lambda(q^2 = 0)}. \tag{27}
\end{aligned}$$

3 LCSR for the SCET form factors

In this section, we construct the light-cone sum rules for the effective form factors $\xi_\Lambda(n \cdot p)$, $\Delta \xi_\Lambda^B(u, n \cdot p)$, and $\Delta_i \xi_\Lambda^C(u, n \cdot p)$ appearing in the factorization formulae Eq. (23) and Eq. (24).

We compute $\xi_\Lambda(n \cdot p)$ and $\Delta \xi_\Lambda^B(u, n \cdot p)$ at one-loop accuracy, while $\Delta_i \xi_\Lambda^C(u, n \cdot p)$ is evaluated at tree level. To this end, we first derive the soft-collinear factorization theorems for the vacuum-to- Λ_b -baryon correlation functions, using an interpolating current for the collinear Λ -baryon in combination with A-type or B-type SCET_I operators. The resummation of parametrically large logarithms $\ln(m_b/\Lambda_{\text{QCD}})$ is performed at leading logarithmic (LL) accuracy using the renormalization group (RG) equation formalism. Subsequently, we extend this framework to derive the soft-collinear factorization theorems for the γ^* -to- Λ_b -baryon correlation functions. In this case, the C-type SCET_I operators, combined with the collinear Λ -baryon interpolating current, yield the form factors $\Delta_i \xi_\Lambda^C(u, n \cdot p)$.

We begin with a correlation function, where the Λ baryon in the final state is replaced by an interpolating current that carries the same quantum numbers. We choose

$$J_\Lambda(x) = \epsilon_{ijk} [u^{\text{T},i}(x) C \gamma_5 \not{t} d^j(x)] s^k(x), \quad (28)$$

which is normalized via the matrix element

$$\langle 0 | J_\Lambda(0) | \Lambda(p, s') \rangle = f_\Lambda(\mu) (n \cdot p) u_\Lambda(p, s'). \quad (29)$$

To match the above current onto SCET, the light-quark fields are decomposed into soft and hard-collinear components. The SCET representation of the Λ interpolating current can then be obtained following the prescriptions given in [19]:

$$J_\Lambda = J_\Lambda^{(0)} + J_\Lambda^{(2)} + J_\Lambda^{(4)} + \dots, \quad (30)$$

where the explicit expressions for the effective currents (noting that there is no soft s -quark field) are given by

$$\begin{aligned} J_\Lambda^{(0)} &= \epsilon_{ijk} [\xi_u^{\text{T},i} C \gamma_5 \not{t} \xi_d^j] \xi_s^k, \\ J_\Lambda^{(2)} &= \epsilon_{ijk} [q_u^{\text{T},i} C \gamma_5 \not{t} \xi_d^j] \xi_s^k - \epsilon_{ijk} [q_d^{\text{T},i} C \gamma_5 \not{t} \xi_u^j] \xi_s^k, \\ J_\Lambda^{(4)} &= \epsilon_{ijk} [q_u^{\text{T},i} C \gamma_5 \not{t} q_d^j] \xi_s^k. \end{aligned} \quad (31)$$

We perform the calculations in the light-cone gauge for both hard-collinear and soft gluon fields. The hard-collinear gluon propagator is given by

$$\langle 0 | T [A_{hc,\mu}^a(x) A_{hc,\nu}^b(y)] | 0 \rangle = \int \frac{d^D l}{(2\pi)^D} \frac{-i \delta^{ab}}{l^2 + i\epsilon} e^{-il \cdot (x-y)} \left[g_{\mu\nu} - \frac{1}{n \cdot l} (l_\mu n_\nu + n_\mu l_\nu) \right]. \quad (32)$$

The multipole-expanded SCET Lagrangian up to $\mathcal{O}(\lambda^2)$ accuracy [33] has been derived using the position-space formalism [19]. To ensure that the correlation function admits a light-cone operator-product expansion (OPE), we assign p_μ as a hard-collinear momentum with

$$n \cdot p \simeq \frac{M_{\Lambda_b}^2 - q^2}{M_{\Lambda_b}} \simeq 2E_\Lambda, \quad |\bar{n} \cdot p| \sim \mathcal{O}(\Lambda_{\text{QCD}}), \quad p^2 < 0. \quad (33)$$

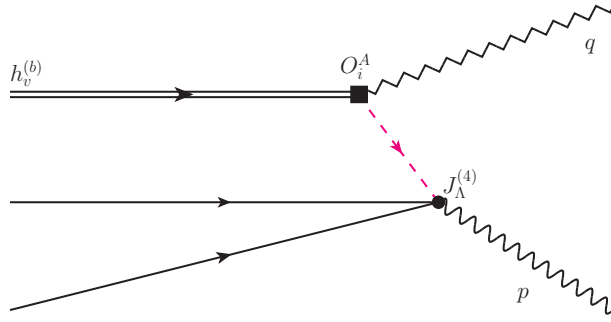


Figure 2: Diagrammatic representation of the correlation function $\Pi_{\text{OPE}}^A(\bar{n} \cdot p)$ at tree level, where the black square denotes the weak transition vertex and the black blob represents the Dirac structure of the Λ -baryon current. The double line indicates the b -quark in HQET; the strange quark is shown by a pink line, and the soft quarks by solid black lines. In addition, hard-collinear propagators are represented by dashed lines. .

3.1 LCSR for A-type soft form factor

We now define the correlation function between the A-type weak decay current and the interpolating current J_Λ ,

$$\Pi^A(\bar{n} \cdot p) \equiv i \int d^4x e^{ip \cdot x} \langle 0 | T [J_\Lambda(x), O_i^A] | \Lambda_b(v, s) \rangle, \quad (34)$$

where $O_i^A = \bar{\xi}_s(0) \Gamma_i^A h(0)$. On the hadronic side, this correlation function is evaluated by inserting a complete set of intermediate states with the same quantum numbers as the Λ baryon:

$$\begin{aligned} \Pi^A|_{\text{res.}} &= \sum_{s'} \frac{\langle 0 | J_\Lambda | \Lambda(p, s') \rangle \langle \Lambda(p, s') | O_i^A | \Lambda_b(v, s) \rangle}{m_\Lambda^2 - p^2} + \dots \\ &= \frac{(n \cdot p) f_\Lambda(\nu) \xi_\Lambda(n \cdot p)}{m_\Lambda^2 - (n \cdot p)(\bar{n} \cdot p)} \sum_{s'} u_\Lambda(p, s') \bar{u}_\Lambda(p, s') \Gamma_i^A u_{\Lambda_b}(v, s) + \dots \\ &= \frac{(n \cdot p) f_\Lambda(\nu) \xi_\Lambda(n \cdot p)}{m_\Lambda^2 / (n \cdot p) - (\bar{n} \cdot p)} \frac{\not{n}}{2} \Gamma_i^A u_{\Lambda_b}(v, s) + \dots, \end{aligned} \quad (35)$$

where the ellipsis denotes contributions from excited and continuum states.

On the other hand, within our selected momentum region, where the light-cone operator-product expansion is applicable, the time-ordered product of the two currents can be computed using perturbation theory. In SCET terminology, by matching from SCET_I to HQET [30, 31, 34], we obtain the hard-collinear-scale jet function, while retaining only the matrix elements of soft fields, which correspond to the Λ_b LCDA.

3.1.1 Correlation function at tree level

At tree level, as shown in Fig. 2, with $\omega_{1,2} = \bar{n} \cdot k_{1,2}$ corresponding to the light-cone momenta of the up- and down-quarks, the correlation function takes the following form:

$$\Pi_{\text{OPE}}^{A, \text{LO}}(\bar{n} \cdot p) \equiv i \int d^4x e^{ip \cdot x} \langle 0 | T [J_\Lambda^{(4)}(x), O_i^A] | \Lambda_b(v, s) \rangle$$

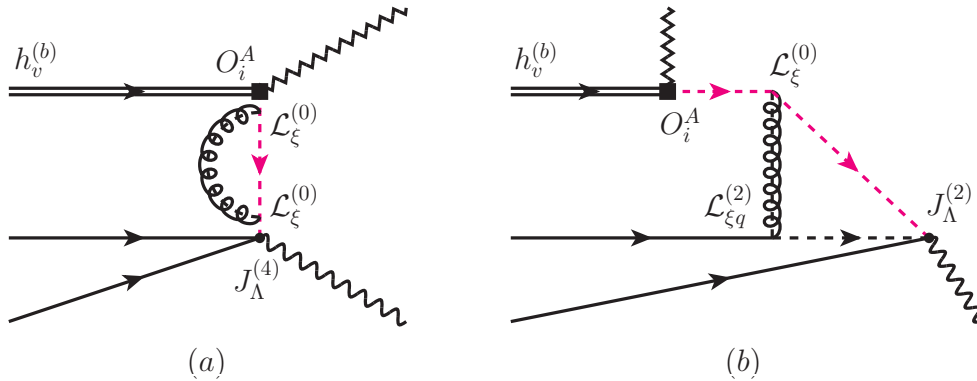


Figure 3: Diagrammatic representation of the non-vanishing one-loop contribution to $\Pi_{\text{OPE}}^A(\bar{n} \cdot p)$ at leading power.

$$\begin{aligned}
&= \int d\omega_1 d\omega_2 F^{(0)}(\omega_1, \omega_2) \\
&= f_{\Lambda_b}^{(2)} \int_0^\infty \frac{d\omega \tilde{\phi}_4(\omega)}{\omega - \bar{n} \cdot p - i\epsilon} \frac{\not{n}}{2} \Gamma_i^A u_{\Lambda_b}(v, s), \tag{36}
\end{aligned}$$

where we have defined

$$\omega = \omega_1 + \omega_2, \tag{37}$$

$$F^{(0)}(\omega_1, \omega_2) = f_{\Lambda_b}^{(2)} \frac{\phi_4(\omega_1, \omega_2)}{\omega - \bar{n} \cdot p - i\epsilon} \frac{\not{n}}{2} \Gamma_i^A u_{\Lambda_b}(v, s), \tag{38}$$

$$\tilde{\phi}_4(\omega) = \omega \int_0^1 du \phi_4(u\omega, (1-u)\omega). \tag{39}$$

The jet function at tree level is simply unity. To obtain this result, we have employed the momentum-space projector for the heavy Λ_b baryon, based on the definition of its light-cone distribution amplitudes as derived in Appendix A. The SCET tree-level result is in exact agreement with the full QCD computation presented in [14, 15].

3.1.2 Factorization of the correlation function at $\mathcal{O}(\alpha_s)$

We now proceed to determine the NLO contribution to the jet function by expanding the matching condition to $\mathcal{O}(\alpha_s)$ accuracy. To this end, we evaluate the one-loop SCET_I diagrams using the subleading power SCET Feynman rules collected in Ref. [35].

There are only two one-loop diagrams in the light-cone gauge [30, 31]. The first corresponds to the interpolating current $J_\Lambda^{(4)}$ combined with the leading-power SCET Lagrangian $\mathcal{L}_\xi^{(0)}$, shown as diagram (a) in Fig. 3. The second involves the interpolating current $J_\Lambda^{(2)}$ and the power-suppressed SCET Lagrangian $\mathcal{L}_{\xi q}^{(2)}$, depicted as diagram (b) in Fig. 3. Both diagrams contribute at the same power as the tree-level result.

For diagram (a) in Fig. 3, the correlation function takes the following form:

$$\begin{aligned}
\Pi_{\text{OPE},(a)}^{\text{A,NLO}}(\bar{n} \cdot p) &= i \int d^4x \int d^4y \int d^4z e^{ip \cdot x} \langle 0 | T \left[J_\Lambda^{(4)}(x) i\mathcal{L}_{\xi_s}^{(0)}(y) i\mathcal{L}_{\xi_s}^{(0)}(z) O_i^A \right] | \Lambda_b(v, s) \rangle \\
&= \int d\omega_1 d\omega_2 F^{(0)}(\omega_1, \omega_2) \frac{\alpha_s C_F}{4\pi} \left[\frac{4}{\epsilon^2} + \frac{1}{\epsilon} \left(4 \ln \frac{\mu^2}{n \cdot p (\omega - \bar{n} \cdot p)} + 3 \right) \right]
\end{aligned}$$

$$+ 2 \ln^2 \frac{\mu^2}{n \cdot p (\omega - \bar{n} \cdot p)} + 3 \ln \frac{\mu^2}{n \cdot p (\omega - \bar{n} \cdot p)} - \frac{\pi^2}{3} + 7 \Big], \quad (40)$$

where the loop integration is performed in $D = 4 - 2\epsilon$ dimensions. Notably, this diagram shares the same loop structure as the meson case, and we therefore expect the perturbative function to match that of the corresponding diagram in the $B \rightarrow P, V$ transitions. Our calculation confirms that the result for Λ_b baryon decay is indeed consistent with the B meson case, as presented in [30, 36].

For diagram (b) in Fig. 3, we consider the contribution of a hard-collinear gluon attached to either the d or the u quark (assuming isospin symmetry). The correlation function then takes the form:

$$\begin{aligned} \Pi_{\text{OPE,(b)}}^{\text{A,NLO}}(\bar{n} \cdot p) &= i \int d^4x \int d^4y \int d^4z e^{ip \cdot x} \langle 0 | T \left[J_\Lambda^{(2)}(x) i\mathcal{L}_{\xi q}^{(2)}(y) i\mathcal{L}_{\xi s}^{(0)}(z) O_i^A \right] | \Lambda_b(v, s) \rangle \\ &= -i g_s^2 C_F \epsilon_{ijk} \int d\omega_1 \int d\omega_2 \int \frac{d^D l}{(2\pi)^D} \int \frac{d^D L}{(2\pi)^D} \times \\ &\quad \frac{n \cdot L \ n \cdot (p - L) \ n \cdot (p - L + l)}{[L^2 + i0][(p - k_1 - L)^2 + i0][(p - k_1 - L + l)^2 + i0][l^2 + i0]} \times \\ &\quad \langle 0 | \bar{q}_u^{\text{T},i}(\omega_1) C \gamma_5 \not{n} \frac{\not{l}}{2} \left[\frac{\not{l}}{2} (\bar{n}^\mu + \frac{\not{L}_\perp}{n \cdot L} \gamma_\perp^\mu) + \gamma_\perp^\mu k_{2\perp\beta} \partial_\perp^\beta \right] \times \\ &\quad (2\pi)^4 \delta^4(l + k_2 - L) q_d^j(\omega_2) \left[g_{\mu\nu} - \frac{1}{n \cdot l} (l_\mu n_\nu + n_\mu l_\nu) \right] \times \\ &\quad \left[\bar{n}^\nu - \frac{\not{L}_\perp \gamma_\perp^\nu}{n \cdot (p - L)} + \frac{\gamma_\perp^\nu (\not{l}_\perp - \not{L}_\perp)}{n \cdot (p - L + l)} \right] \frac{\not{n}}{2} \Gamma_i^A h^k(0) | \Lambda_b(v, s) \rangle, \end{aligned} \quad (41)$$

which can be evaluated using three distinct methods by identifying the transverse derivative ∂_\perp^β acting on the Dirac delta function as $\partial/\partial k_{2\perp\beta}$, $\partial/\partial L_{\perp\beta}$, or $\partial/\partial l_{\perp\beta}$, respectively [35]. We have explicitly verified that all three approaches yield the same result:

$$\begin{aligned} \Pi_{\text{OPE,(b)}}^{\text{A,NLO}}(\bar{n} \cdot p) &= \int d\omega_1 d\omega_2 F^{(0)}(\omega_1, \omega_2) \frac{\alpha_s C_F}{4\pi} \left\{ -\frac{2}{\epsilon^2} - \frac{1}{\epsilon} \left[2 \ln \frac{\mu^2}{n \cdot p (\omega - \bar{n} \cdot p)} \right. \right. \\ &\quad \left. \left. + 2 \ln \frac{\omega - \bar{n} \cdot p}{\omega_1 - \bar{n} \cdot p} + \frac{7}{2} \right] - \ln^2 \frac{\mu^2}{n \cdot p (\omega - \bar{n} \cdot p)} - \frac{7}{2} \ln \frac{\mu^2}{n \cdot p (\omega - \bar{n} \cdot p)} \right. \\ &\quad \left. - 2 \ln \frac{\omega - \bar{n} \cdot p}{\omega_1 - \bar{n} \cdot p} \ln \frac{\mu^2}{n \cdot p (\omega - \bar{n} \cdot p)} - \ln^2 \frac{\omega - \bar{n} \cdot p}{\omega_1 - \bar{n} \cdot p} \right. \\ &\quad \left. + \left(2 \frac{\omega_1 - \bar{n} \cdot p}{\omega_2} - \frac{3}{2} \right) \ln \frac{\omega - \bar{n} \cdot p}{\omega_1 - \bar{n} \cdot p} + \frac{\pi^2}{6} - \frac{15}{2} \right\}, \end{aligned} \quad (42)$$

where we have employed the Wandzura-Wilczek approximation as given in Eq. (92).

3.1.3 Leading power contribution

The tree-level and one-loop contributions to the A-type correlation function are formally suppressed by λ^2 compared to the leading-power contribution, which begins at the two-loop level. It is justified to neglect the leading-power contribution in our analysis. This conclusion is consistent with [37], which observes that the numerical value of the leading-power form factor is approximately one order of magnitude smaller than that governed by soft processes.

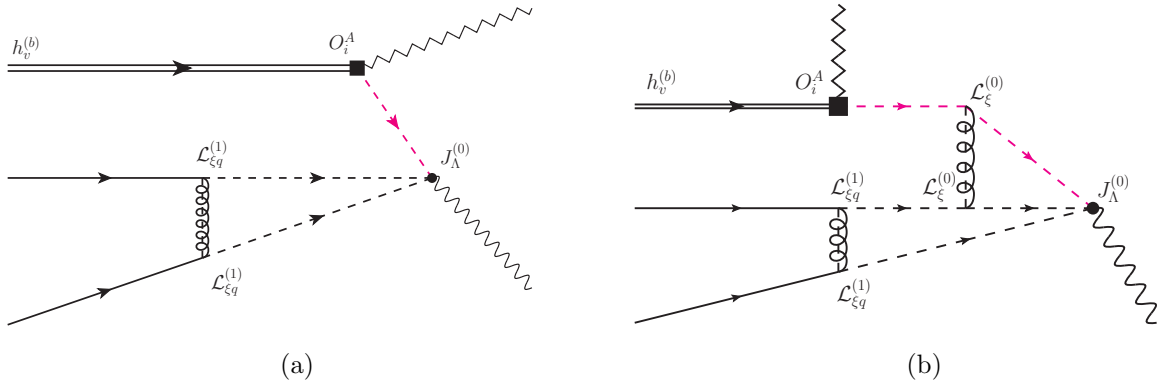


Figure 4: Diagram (a) shows the leading-power one-loop representation of $\Pi_{\text{OPE}}^{\text{A}}(\bar{n} \cdot p)$, while diagram (b) illustrates a possible leading-power two-loop contribution to $\Pi_{\text{OPE}}^{\text{A}}(\bar{n} \cdot p)$.

For the leading-power contribution, the interpolating current is $J_{\Lambda}^{(0)}$. At one-loop level, there are two soft-collinear interactions $\mathcal{L}_{\xi q}^{(1)}$ that convert the u and d quarks in $J_{\Lambda}^{(0)}$ from hard-collinear to soft via the exchange of a hard-collinear gluon, as illustrated in Fig. 4a,

$$\Pi_0^{\text{A}} \equiv i \int d^4x \int d^4y \int d^4z e^{ip \cdot x} \langle 0 | T \left[i \mathcal{L}_{\xi u q u}^{(1)}(y) i \mathcal{L}_{\xi d q d}^{(1)}(z) J_{\Lambda}^{(0)}(x) O_i^{\text{A}} \right] | \Lambda_b(v, s) \rangle. \quad (43)$$

However, the loop integral of this diagram is scaleless, in agreement with Ref. [15]. Consequently, the leading-power contribution to the A-type correlation function arises at the two-loop level. A schematic diagram in light-cone gauge is shown in Fig. 4b.

3.1.4 Factorization-scale independence

The factorization formula for the A-type correlation function is

$$\begin{aligned} \Pi_{\text{OPE}}^{\text{A}}(\bar{n} \cdot p) &\equiv \Pi_{\text{OPE}}^{\text{A,LO}}(\bar{n} \cdot p) + \Pi_{\text{OPE,(a)}}^{\text{A,NLO}}(\bar{n} \cdot p) + \Pi_{\text{OPE,(b)}}^{\text{A,NLO}}(\bar{n} \cdot p) + \mathcal{O}(\alpha_s^2) \\ &= f_{\Lambda_b}^{(2)}(\mu) \int d\omega_1 d\omega_2 \frac{\phi_4(\omega_1, \omega_2, \mu)}{\omega - \bar{n} \cdot p - i\epsilon} J \left(\frac{\mu^2}{\bar{n} \cdot p \omega_i}, \frac{\omega_i}{\bar{n} \cdot p} \right) \frac{\not{n}}{2} \Gamma_i^{\text{A}} u_{\Lambda_b}(v, s) + \mathcal{O}(\alpha_s^2), \end{aligned} \quad (44)$$

where the jet function is

$$\begin{aligned} J \left(\frac{\mu^2}{\bar{n} \cdot p \omega_i}, \frac{\omega_i}{\bar{n} \cdot p} \right) &= 1 + \frac{\alpha_s(\mu)}{4\pi} C_F \left\{ \ln^2 \frac{\mu^2}{n \cdot p (\omega - \bar{n} \cdot p)} - \frac{1}{2} \ln \frac{\mu^2}{n \cdot p (\omega - \bar{n} \cdot p)} \right. \\ &\quad - 2 \ln \frac{\omega - \bar{n} \cdot p}{\omega_1 - \bar{n} \cdot p} \ln \frac{\mu^2}{n \cdot p (\omega - \bar{n} \cdot p)} - \ln^2 \frac{\omega - \bar{n} \cdot p}{\omega_1 - \bar{n} \cdot p} \\ &\quad \left. + \left(2 \frac{\omega_1 - \bar{n} \cdot p}{\omega_2} - \frac{3}{2} \right) \ln \frac{\omega - \bar{n} \cdot p}{\omega_1 - \bar{n} \cdot p} - \frac{\pi^2}{6} - \frac{1}{2} \right\}. \end{aligned} \quad (45)$$

This result agrees with [15], which calculates the $\Lambda_b \rightarrow \Lambda$ form factors using the method of regions [38, 39].

Having obtained the one-loop factorization formulae, we now explicitly verify the factorization scale independence of the correlation functions $C_i^{\text{A}}(n \cdot p, \mu) \Pi_{\text{OPE}}^{\text{A}}(\bar{n} \cdot p)$ at one loop. The RG equation for the hard function reads

$$\frac{d}{d \ln \mu} C_i^{\text{A}}(n \cdot p, \mu) = \gamma^{\text{A}} C_i^{\text{A}}(n \cdot p, \mu), \quad (46)$$

where [17]

$$\gamma^A = -\Gamma_{\text{cusp}}(\alpha_s) \ln \frac{\mu}{n \cdot p} + \tilde{\gamma}(\alpha_s) = \frac{\alpha_s(\mu)}{4\pi} C_F \left(-4 \ln \frac{\mu}{n \cdot p} - 5 \right) + \mathcal{O}(\alpha_s^2). \quad (47)$$

For the jet function, we find

$$\frac{d}{d \ln \mu} J \left(\frac{\mu^2}{\bar{n} \cdot p \omega_i}, \frac{\omega_i}{\bar{n} \cdot p} \right) = \frac{\alpha_s(\mu)}{4\pi} C_F \left[4 \ln \frac{\mu^2}{n \cdot p (\omega - \bar{n} \cdot p)} - 4 \ln \frac{\omega - \bar{n} \cdot p}{\omega_1 - \bar{n} \cdot p} - 1 \right]. \quad (48)$$

We also obtain the one-loop evolution equation for the Λ_b -baryon DA $\phi_4(\omega_1, \omega_2, \mu)$, which agrees with [15]:

$$\begin{aligned} & \int_0^\infty d\omega_1 \int_0^\infty d\omega_2 \frac{1}{\omega_1 + \omega_2 - \bar{n} \cdot p - i0} \frac{d}{d \ln \mu} \left[f_{\Lambda_b}^{(2)}(\mu) \phi_4(\omega_1, \omega_2, \mu) \right] \\ &= -\frac{\alpha_s(\mu)}{4\pi} C_F \int_0^\infty d\omega_1 \int_0^\infty d\omega_2 \frac{1}{\omega_1 + \omega_2 - \bar{n} \cdot p - i0} \\ & \quad \times \left[4 \ln \frac{\mu}{\omega - \bar{n} \cdot p} - 4 \ln \frac{\omega - \bar{n} \cdot p}{\omega_1 - \bar{n} \cdot p} - 5 \right] \left[f_{\Lambda_b}^{(2)}(\mu) \phi_4(\omega_1, \omega_2, \mu) \right]. \end{aligned} \quad (49)$$

From the above results, we can readily deduce

$$\frac{d}{d \ln \mu} \left[C_i^A(n \cdot p, \mu) \Pi_{\text{OPE}}^A(\bar{n} \cdot p) \right] = -\frac{\alpha_s(\mu)}{4\pi} C_F f_{\Lambda_b}^{(2)}(\mu) \int_0^\infty d\omega_1 \int_0^\infty d\omega_2 \frac{\phi_4(\omega_1, \omega_2, \mu)}{\omega - \bar{n} \cdot p - i0}. \quad (50)$$

The residual μ -dependence in Eq. (50) stems from the ultraviolet renormalization of the baryon current:

$$\frac{d}{d \ln \mu} \ln f_\Lambda(\mu) = - \left(\frac{\alpha_s(\mu)}{4\pi} \right)^k \gamma_\Lambda^{(k)}, \quad (51)$$

with $\gamma_\Lambda^{(1)} = 4/3$ [40, 41]. By distinguishing the renormalization scales for the interpolating current of the Λ -baryon and the weak transition current in QCD from the factorization scale (see the next section for details), we arrive at the conclusion that the factorization-scale dependence cancels completely in the factorized expressions of the correlation functions $C_i^A(n \cdot p, \mu) \Pi_{\text{OPE}}^A(\bar{n} \cdot p)$ at one loop.

3.1.5 LCSR of $\xi_\Lambda(n \cdot p)$ at $\mathcal{O}(\alpha_s)$

The dispersion forms of the correlation functions are derived using spectral representations in Appendix A of Ref. [15]. By comparing the partonic and hadronic representations of the correlation functions, subtracting the continuum-state contributions, and performing a Borel transformation, we obtain the sum rule for the form factor:

$$n \cdot p f_\Lambda(\nu) \exp \left(-\frac{m_\Lambda^2}{n \cdot p \omega_M} \right) \xi_\Lambda(n \cdot p) = f_{\Lambda_b}^{(2)} \int_0^{\omega_s} d\omega' \phi_{4,\text{eff}}(\omega', \mu, \nu) e^{-\omega'/\omega_M}, \quad (52)$$

where ν denotes the renormalization scale of the baryon current. It is evident that the $\ln \nu$ dependence must be separated from the jet function.

The effective ‘‘distribution amplitude’’ $\phi_{4,\text{eff}}(\omega', \mu, \nu)$ is given by

$$\begin{aligned}
\phi_{4,\text{eff}}(\omega', \mu, \nu) &= \tilde{\phi}_4(\omega', \mu) + \frac{\alpha_s(\mu)}{4\pi} C_F \left\{ \int_0^{\omega'} d\omega \left[\frac{2}{\omega - \omega'} \ln \frac{\mu^2}{n \cdot p(\omega' - \omega)} \right]_{\oplus} \tilde{\phi}_4(\omega, \mu) \right. \\
&\quad - 2\omega' \int_0^{\omega'} d\omega \left[\frac{1}{\omega - \omega'} \ln \frac{\omega' - \omega}{\omega'} \right]_{\oplus} \phi_4(\omega, \mu) \\
&\quad - \omega' \int_{\omega'}^{\infty} d\omega \left[\frac{\omega}{\omega'} \ln^2 \frac{\mu^2}{n \cdot p\omega'} - 2 \ln \frac{\mu^2}{n \cdot p\omega'} \ln \frac{\omega - \omega'}{\omega'} - \frac{11}{2} \ln \frac{\omega - \omega'}{\omega'} \right. \\
&\quad \quad \left. - \frac{\pi^2 + 1}{2} \frac{\omega}{\omega'} + \left(\frac{2\pi^2}{3} - \frac{11}{2} \right) \right] \frac{d\phi_4(\omega, \mu)}{d\omega} \\
&\quad - \int_{\omega'}^{\infty} d\omega \left[\ln^2 \frac{\mu^2}{n \cdot p\omega'} + 2 \ln \frac{\omega - \omega'}{\omega} - \frac{\pi^2 + 1}{2} \right] \phi_4(\omega, \mu) \\
&\quad \left. - \int_0^{\omega'} d\omega \left[2 \ln \frac{\mu^2}{n \cdot p(\omega' - \omega)} + \frac{1}{2} \ln \frac{\nu^2}{n \cdot p(\omega' - \omega)} \right] \frac{d\tilde{\phi}_4(\omega, \mu)}{d\omega} \right\}, \quad (53)
\end{aligned}$$

where the Λ_b -baryon DA $\phi_4(\omega_1, \omega_2, \mu)$ is abbreviated as $\phi_4(\omega, \mu)$ for brevity, since

$$\phi_4(\omega_1, \omega_2, \mu) = \phi_4(u\omega, (1-u)\omega, \mu)$$

is assumed to be independent of the momentum fraction u , as motivated by Refs. [14, 42, 43]. Within this approximation, $\tilde{\phi}_4(\omega, \mu)$ is given by

$$\tilde{\phi}_4(\omega, \mu) = \omega \int_0^1 du \phi_4(u\omega, (1-u)\omega, \mu) = \omega \phi_4(\omega, \mu).$$

The \oplus function is defined as

$$\int_0^{\infty} d\omega [f(\omega, \omega')]_{\oplus} g(\omega) = \int_0^{\infty} d\omega f(\omega, \omega') [g(\omega) - g(\omega')]. \quad (54)$$

From Eq. (52), we can derive the scaling law for the ‘‘soft’’ form factor:

$$\xi_{\Lambda}(n \cdot p) \sim \lambda^6. \quad (55)$$

It is suppressed by λ^2 compared to the leading-power form factors, which is consistent with the results in Ref. [37].

3.2 LCSR for B-type form factor

We now define the correlation function between the B-type weak decay current and the interpolating current J_{Λ} to extract the non-local form factor $\Delta\xi_{\Lambda}^B(u, n \cdot p)$, which corresponds to the hard-scattering corrections discussed in Ref. [14]. Accordingly, we define

$$\Pi^B(u, \bar{n} \cdot p) \equiv i n \cdot p \int d^4x e^{ip \cdot x} \int \frac{da}{2\pi} e^{-iun \cdot pa} \langle 0 | T [J_{\Lambda}(x), O_j^B(a)] | \Lambda_b(v, s) \rangle, \quad (56)$$

with $O_j^B(a) = \bar{\xi}_s(0) \Gamma_j^B A_{hc\perp}^{\nu}(an) h(0)$.

Due to the isospin symmetry of the strong interaction, there is only one contributing diagram at $\mathcal{O}(\alpha_s)$, as shown in Fig. 5. By exchanging a hard-collinear gluon, the relevant

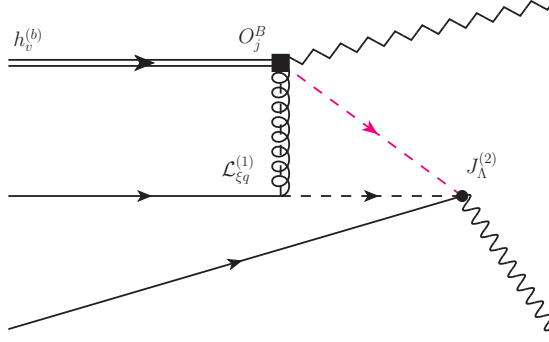


Figure 5: Diagrammatic representation of the leading-power $\Pi_{\text{OPE}}^{\text{B}}(u, \bar{n} \cdot p)$ at leading order.

ingredients are the interpolating current $J_{\Lambda}^{(2)}$ and the subleading-power SCET Lagrangian $\mathcal{L}_{\xi_q}^{(1)}$. Owing to the additional A_{hc}^{\perp} field in $O_j^B(a)$, this correlation function is of the same power as the A-type correlation functions, and takes the following form:

$$\begin{aligned} \Pi_{\text{OPE}}^{\text{B,LO}}(u, \bar{n} \cdot p) &= i n \cdot p \int d^4x e^{ip \cdot x} \int d^4y \int \frac{da}{2\pi} e^{-iun \cdot pa} \\ &\times \langle 0 | T [J_{\Lambda}^{(2)}(x), i\mathcal{L}_{\xi_q}^{(1)}(y), O_j^B(a)] | \Lambda_b(v, s) \rangle. \end{aligned} \quad (57)$$

This correlation function vanishes due to rotational invariance in the transverse plane (which implies an odd number of γ_{\perp} matrices in the trace over spinor space). This is why the insertion of $\mathcal{L}_{\xi_q}^{(1)}$ yields a vanishing contribution in diagram (b) of Fig. 3 [31]. In Ref. [14], this diagram is evaluated using the full momentum in the numerator of the hard-collinear quark propagators, while employing the light-cone projector to preserve rotational invariance in the transverse plane. According to their procedure, only the subleading transverse momentum components in the numerators of the hard-collinear s -quark and u (d)-quark propagators contribute. This implies that their $\Delta\xi_{\Lambda}$ is formally λ^2 (α_s)-suppressed relative to the soft form factor ξ_{Λ} . This power counting is consistent with their numerical result $\Delta\xi_{\Lambda}/\xi_{\Lambda} \simeq -0.8\%$.

3.3 LCSR for C-type non-factorisable contributions

The C-type annihilation operator corresponds to the non-factorizable contribution [15, 21, 32]. For convenience, we define new operators $O_{\pm}^C(a)$ with explicit colour indices as:

$$O_{\pm}^C(a) = \bar{\xi}_s^{k_1}(0)(1 + \gamma_5)\gamma_{\perp}^{\mu} h^{k_2}(0) \bar{\xi}_q^{l_1}(an)\gamma_{\mu}^{\perp}(1 \pm \gamma_5)\chi_q^{l_2}(0). \quad (58)$$

The C-type γ^* -to- Λ_b -baryon correlation function is defined as

$$\begin{aligned} \Pi^{\text{C},i}(u, \bar{n} \cdot p) &\equiv i n \cdot p \int d^4x e^{ip \cdot x} \int \frac{da}{2\pi} e^{-iun \cdot pa} \langle \gamma^*(q, \lambda) | T [J_{\Lambda}(x), Q_i^C(0, a, 0)] | \Lambda_b(v, s) \rangle, \\ \Pi^{\text{C},\pm}(u, \bar{n} \cdot p) &\equiv i n \cdot p \int d^4x e^{ip \cdot x} \int \frac{da}{2\pi} e^{-iun \cdot pa} \langle \gamma^*(q, \lambda) | T [J_{\Lambda}(x), O_{\pm}^C(a)] | \Lambda_b(v, s) \rangle. \end{aligned} \quad (59)$$

Then we have the following relations:

$$\begin{aligned} \Pi^{\text{C},1}(u, \bar{n} \cdot p) &= \delta_{k_1 k_2} \delta_{l_1 l_2} \Pi^{\text{C},-}(u, \bar{n} \cdot p), & \Pi^{\text{C},2}(u, \bar{n} \cdot p) &= \delta_{k_1 l_2} \delta_{l_1 k_2} \Pi^{\text{C},-}(u, \bar{n} \cdot p), \\ \Pi^{\text{C},3}(u, \bar{n} \cdot p) &= \delta_{k_1 k_2} \delta_{l_1 l_2} \Pi^{\text{C},+}(u, \bar{n} \cdot p), & \Pi^{\text{C},4}(u, \bar{n} \cdot p) &= \delta_{k_1 l_2} \delta_{l_1 k_2} \Pi^{\text{C},+}(u, \bar{n} \cdot p). \end{aligned} \quad (60)$$

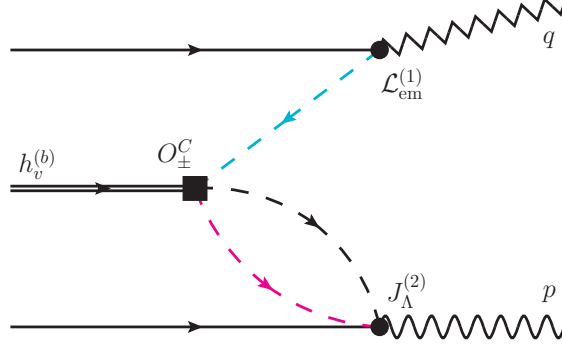


Figure 6: Diagrammatic representation of the leading-power $\Pi_{\text{OPE}}^{\text{C},\pm}(u, \bar{n} \cdot p)$ at leading order. Blue dashed line indicate anti-hard-collinear propagator.

On the hadronic side, the contribution of the Λ baryon to the correlation function is given by

$$\begin{aligned} \Pi^{\text{C},i}|_{\text{res.}} &\simeq n \cdot p \int \frac{da}{2\pi} e^{-iu n \cdot p a} \sum_{s'} \frac{\langle 0 | J_{\Lambda} | \Lambda(p, s') \rangle \langle \Lambda(p, s') | \gamma^*(q, \lambda) | Q_i^{\text{C}}(0, a, 0) | \Lambda_b(v, s) \rangle}{m_{\Lambda}^2 - p^2} \\ &= g_{\text{em}} M_{\Lambda_b}^2 \bar{\epsilon}_{\nu}^*(q, \lambda) \Delta_i \xi_{\Lambda}^{\text{C}}(u, n \cdot p) \frac{(n \cdot p) f_{\Lambda}(v)}{m_{\Lambda}^2 / (n \cdot p) - (\bar{n} \cdot p)} \frac{\not{n}}{2} (1 + \gamma_5) \gamma_{\perp}^{\nu} u_{\Lambda_b}(v, s). \end{aligned} \quad (61)$$

On the partonic side, the OPE of $\Pi^{\text{C},i}(u, \bar{n} \cdot p)$ is obtained via the relation in Eq. (60). By applying isospin symmetry of the strong interaction, only one diagram appears at leading order, as shown in Fig. 6, where the photon is emitted from a spectator quark. The relevant components are the interpolating current $J_{\Lambda}^{(2)}$ and the subleading-power SCET electromagnetic Lagrangian:

$$\mathcal{L}_{\text{em}}^{(1)} = g_{\text{em}} \sum_q Q_q \bar{\chi}_q A_{hc\perp}^{(\text{em})} q_q, \quad (62)$$

where Q_q is the electric charge of the quark q . Inserting the effective electromagnetic interaction vertex yields the following expression for Fig. 6:

$$\begin{aligned} \Pi_{\text{OPE}}^{\text{C},\pm}(u, \bar{n} \cdot p) &= i n \cdot p \int d^4x e^{ip \cdot x} \int d^4y \int \frac{da}{2\pi} e^{-iu n \cdot p a} \times \\ &\quad \langle \gamma^*(q, \lambda) | T \left[J_{\Lambda}^{(2)}(x), O_{\pm}^{\text{C}}(a), i\mathcal{L}_{\text{em}}^{(1)}(y) \right] | \Lambda_b(v, s) \rangle \\ &= i g_{\text{em}} Q_u \bar{\epsilon}_{\nu}^*(q, \lambda) \epsilon_{i l k_1} \int d\bar{\omega}_1 \frac{1}{n \cdot q - \bar{\omega}_1} \int d\omega_2 \times \\ &\quad \int \frac{d^D l}{(2\pi)^D} \delta \left(u - \frac{n \cdot l}{n \cdot p} \right) \frac{n \cdot l}{l^2 + i0} \frac{n \cdot (p - l)}{(p - l)^2 - n \cdot (p - l) \omega_2 + i0} \times \\ &\quad \langle 0 | \left[\bar{q}_d^{\text{T},i}(\omega_2) C \gamma_5 \not{n} \frac{\not{n}}{2} \gamma_{\perp}^{\mu} (1 \pm \gamma_5) \frac{\not{n}}{2} \gamma_{\perp}^{\nu} q_u^{\text{L}}(\bar{\omega}_1) \right] \frac{\not{n}}{2} \gamma_{\mu}^{\perp} (1 - \gamma_5) h^{k_2}(0) | \Lambda_b(v, s) \rangle, \end{aligned} \quad (63)$$

where $\bar{\omega}_1 = n \cdot k_1$ and $\omega_2 = \bar{n} \cdot k_2$. For clarity, we have focused on the scenario where the photon is emitted from the u quark. Owing to isospin symmetry, the results for photon emission from the d quark are identical, with the only modification being the substitution $Q_u \rightarrow Q_d$, as we disregard the masses of the light quarks [21].

Since the LCSRs are derived using a dispersion relation of the form

$$\Pi_{\text{OPE}}^{\text{C},\pm}(u, \bar{n} \cdot p) = \frac{1}{\pi} \int_0^\infty d\omega \frac{\text{Im} \Pi_{\text{OPE}}^{\text{C},\pm}(u, \omega)}{\omega - \bar{n} \cdot p - i\epsilon}, \quad (64)$$

we only require the imaginary part of the correlator. The loop integration yields

$$\begin{aligned} & i \mu^{4-D} \int \frac{d^D l}{(2\pi)^D} \delta\left(u - \frac{n \cdot l}{n \cdot p}\right) \frac{n \cdot l}{l^2 + i0} \frac{n \cdot (p-l)}{(p-l)^2 - n \cdot (p-l)\omega_2 + i0} \\ &= -\frac{1}{16\pi^2} u \bar{u} \theta(u) \theta(\bar{u}) (n \cdot p)^2 \left[\frac{1}{\epsilon} + \ln\left(\frac{-\mu^2}{n \cdot p (\bar{n} \cdot p - \omega_2)}\right) - \ln(u \bar{u}) \right]. \end{aligned} \quad (65)$$

Then, we obtain the imaginary part of the correlation function:

$$\begin{aligned} \text{Im} \Pi_{\text{OPE}}^{\text{C},\pm}(u, \omega) &= \frac{1}{16\pi} g_{\text{em}} Q_u \bar{e}_\nu^*(q, \lambda) u \bar{u} \theta(u) \theta(\bar{u}) (n \cdot p)^2 \int d\bar{\omega}_1 \int d\omega_2 \frac{\theta(\omega - \omega_2)}{n \cdot q - \bar{\omega}_1} \times \\ & \epsilon_{i_1 k_1} \langle 0 | [\bar{q}_u^{\text{T}, l_2}(\bar{\omega}_1) C \gamma_\perp^\nu \not{n} (1 \pm \gamma_5) \gamma_\perp^\mu \gamma_5 q_d^i(\omega_2)] \frac{\not{n}}{2} \gamma_\mu^\perp (1 - \gamma_5) h^{k_2}(0) | \Lambda_b(v, s) \rangle. \end{aligned} \quad (66)$$

The above expression depends on two opposite light-cone projections of the light-quark momenta in the Λ_b baryon, requiring the momentum-space projector $M^{(2)}(\bar{\omega}_1, \omega_2)$ defined in Eq. (103). We then obtain:

$$\begin{aligned} \text{Im} \Pi_{\text{OPE}}^{\text{C},1}(u, \omega) &= -\frac{1}{8\pi} g_{\text{em}} Q_u f_{\Lambda_b}^{(2)} \bar{e}_\nu^*(q, \lambda) u \bar{u} \theta(u) \theta(\bar{u}) (n \cdot p)^2 \int d\bar{\omega}_1 \int d\omega_2 \frac{\theta(\omega - \omega_2)}{n \cdot q - \bar{\omega}_1} \times \\ & \left(\chi_2(\bar{\omega}_1, \omega_2) + \chi_{42}^{(ii)}(\bar{\omega}_1, \omega_2) \right) \left(\frac{g_\perp^{\nu\mu}}{2} - \frac{i\epsilon^{\perp\nu\perp\mu\{n\}}}{4} \right) \frac{\not{n}}{2} \gamma_\mu^\perp (1 - \gamma_5) u_{\Lambda_b}(v, s), \\ \text{Im} \Pi_{\text{OPE}}^{\text{C},3}(u, \omega) &= -\frac{1}{8\pi} g_{\text{em}} Q_u f_{\Lambda_b}^{(2)} \bar{e}_\nu^*(q, \lambda) u \bar{u} \theta(u) \theta(\bar{u}) (n \cdot p)^2 \int d\bar{\omega}_1 \int d\omega_2 \frac{\theta(\omega - \omega_2)}{n \cdot q - \bar{\omega}_1} \times \\ & \left(\chi_2(\bar{\omega}_1, \omega_2) + \chi_{42}^{(ii)}(\bar{\omega}_1, \omega_2) \right) \left(\frac{g_\perp^{\nu\mu}}{2} + \frac{i\epsilon^{\perp\nu\perp\mu\{n\}}}{4} \right) \frac{\not{n}}{2} \gamma_\mu^\perp (1 - \gamma_5) u_{\Lambda_b}(v, s). \end{aligned} \quad (67)$$

The color structure leads to the relations:

$$\text{Im} \Pi_{\text{OPE}}^{\text{C},1}(u, \omega) = -\text{Im} \Pi_{\text{OPE}}^{\text{C},2}(u, \omega), \quad \text{Im} \Pi_{\text{OPE}}^{\text{C},3}(u, \omega) = -\text{Im} \Pi_{\text{OPE}}^{\text{C},4}(u, \omega). \quad (68)$$

In our convention, $\gamma_5 = i\gamma^0\gamma^1\gamma^2\gamma^3$. For the Levi-Civita symbol, we use $\epsilon^{0123} = 1$, and adopt the shorthand notation $\epsilon^{\mu\nu\rho\sigma} q_\sigma \equiv \epsilon^{\mu\nu\rho\{q\}}$. In $D = 4$ dimensions, the following identities hold:

$$\begin{aligned} & \left(\frac{g_\perp^{\nu\mu}}{2} - \frac{i\epsilon^{\perp\nu\perp\mu\{n\}}}{4} \right) \frac{\not{n}}{2} \gamma_\mu^\perp (1 - \gamma_5) = 0, \\ & \left(\frac{g_\perp^{\nu\mu}}{2} + \frac{i\epsilon^{\perp\nu\perp\mu\{n\}}}{4} \right) \frac{\not{n}}{2} \gamma_\mu^\perp (1 - \gamma_5) = \frac{\not{n}}{2} \gamma_\perp^\nu (1 - \gamma_5), \end{aligned} \quad (69)$$

which lead to the final results:

$$\begin{aligned} \Delta_1 \xi_\Lambda^C(u, n \cdot p) &= \Delta_2 \xi_\Lambda^C(u, n \cdot p) = 0, \\ \Delta_3 \xi_\Lambda^C(u, n \cdot p) &= -\Delta_4 \xi_\Lambda^C(u, n \cdot p) = -\Delta \xi_\Lambda^C(u, n \cdot p). \end{aligned} \quad (70)$$

The sum rules for the C-type form factors are

$$\Delta\xi_\Lambda^C(u, n \cdot p) = \frac{f_{\Lambda_b}^{(2)}}{f_\Lambda(\nu)} \frac{Q_u + Q_d}{8\pi^2} \frac{n \cdot p}{M_{\Lambda_b}^2} u\bar{u} \theta(u)\theta(\bar{u}) \times \int_0^{\omega_s} d\omega \int_0^\omega d\omega_2 \int_0^\infty d\bar{\omega}_1 \frac{\chi_2(\bar{\omega}_1, \omega_2) + \chi_{42}^{(ii)}(\bar{\omega}_1, \omega_2)}{n \cdot q - \bar{\omega}_1 + i\epsilon} \exp\left(\frac{m_\Lambda^2 - n \cdot p \omega}{n \cdot p \omega_M}\right). \quad (71)$$

Our result agrees with Ref. [21] up to a sign difference.² From Eq. (71), we can derive the scaling law for C-type form factors:

$$\Delta_3\xi_\Lambda^C(u, n \cdot p) \sim \Delta_4\xi_\Lambda^C(u, n \cdot p) \sim \lambda^6, \quad (72)$$

while $\Delta_1\xi_\Lambda^C(u, n \cdot p) = \Delta_2\xi_\Lambda^C(u, n \cdot p) = 0$ at $\mathcal{O}(\lambda^6)$. From the above analysis, the relation in Eq. (27) reduces to:

$$\begin{aligned} \Delta C_1^A(q^2) &= 16\pi^2 \frac{\alpha_e}{4\pi} \frac{1}{q^2} M_{\Lambda_b}^2 \int du [C_3^C - C_4^C] (n \cdot p, \bar{u}) \frac{\Delta\xi_\Lambda^C(u, n \cdot p)}{\xi_\Lambda(n \cdot p)}, \\ \Delta C_\gamma^A(q^2 = 0) &= -g_{\text{em}} M_{\Lambda_b}^2 \int du [C_3^C - C_4^C] (n \cdot p, \bar{u}) \frac{\Delta\xi_\Lambda^C(u, q^2 = 0)}{\xi_\Lambda(q^2 = 0)}. \end{aligned} \quad (73)$$

4 Numerical results

Having established the SCET sum rules for the $\Lambda_b \rightarrow \Lambda$ form factor, we are now ready to investigate their phenomenological implications. We begin the numerical analysis by specifying the non-perturbative models for the Λ_b -baryon LCDA, determining the sum rule parameters, and evaluating the normalization constants $f_\Lambda(\nu)$ and $f_{\Lambda_b}^{(2)}(\mu)$. Finally, we present theoretical predictions for the $\Lambda_b \rightarrow \Lambda$ form factor at large hadronic recoil.

4.1 Input parameters

The LCDA of the Λ_b baryon is derived in Appendix A. For our numerical calculations, we adopt the exponential model specified in Eq. (95). In the context of the soft form factor, only the partially integrated function $\phi_4(\omega)$ contributes, and it takes a simple form at the soft scale:

$$\phi_4(\omega, \mu_0) := \frac{1}{\omega_0^2} e^{-\omega/\omega_0}.$$

Using the matching procedure from Ref. [15], we take

$$\xi_\Lambda^{\text{NLO}}(q^2 = 0) \simeq f_{\Lambda_b \rightarrow \Lambda}^+(0) = 0.18 \pm 0.04$$

as input to determine $\omega_0 = 430_{-50}^{+70}$ MeV. We then illustrate the effective ‘‘distribution amplitude’’ $\phi_{4,\text{eff}}(\omega', \mu, \nu)$ in Eq. (53) using this model in Fig. 7, with the central value $\omega_0 = 0.430$ GeV. The blue dashed and red solid curves correspond to the sum rule predictions at LO and NLO, respectively.

Regarding the determination of the sum rule parameters, we follow the strategies proposed for studying the sum rules of the $B \rightarrow \pi$ form factors [34].

²A minus sign appears to be missing in Eq.(3.32) of Ref. [21].

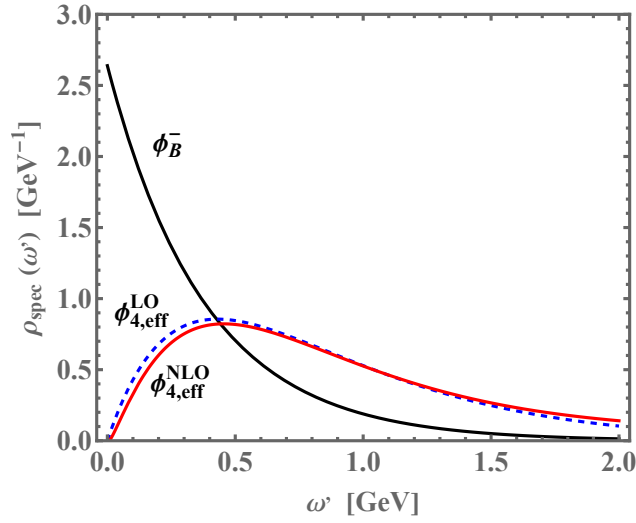


Figure 7: Spectral functions correspond to sum rules for the $B \rightarrow \pi$ form factors and ξ_Λ for $\Lambda_b \rightarrow \Lambda$. The black solid curves represent the LO sum rule for the $B \rightarrow \pi$ form factors, which is simply $\phi_B^-(\omega', 1.5)$. The blue dashed and red solid curves show the LO and NLO sum rules for ξ_Λ , corresponding to $\phi_{4,\text{eff}}^{\text{LO}}(\omega', 1.5, 1.5)$ and $\phi_{4,\text{eff}}^{\text{NLO}}(\omega', 1.5, 1.5)$, respectively, with the central value $\omega_0 = 0.430$.

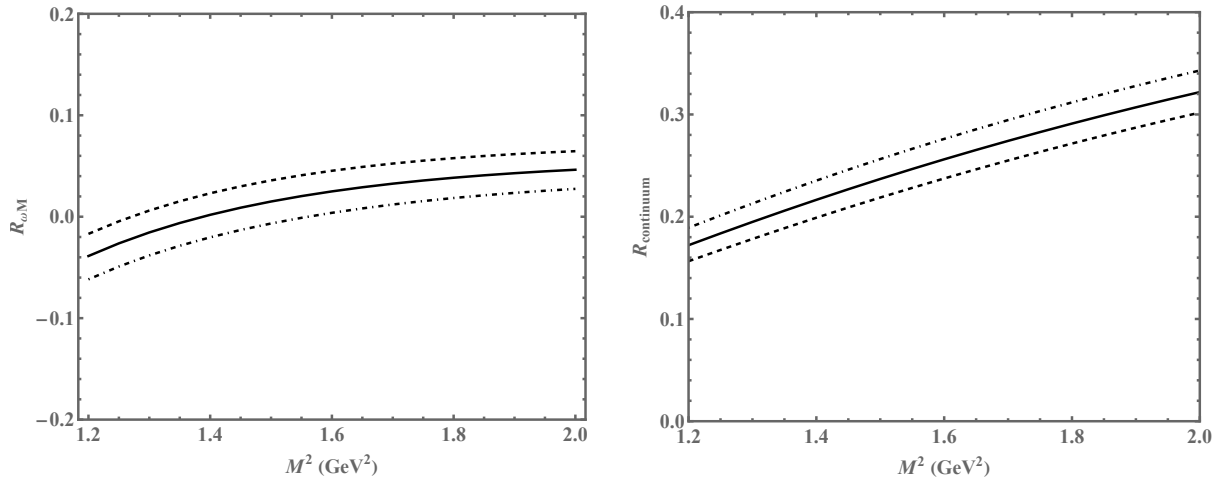


Figure 8: Dependence of R_{ω_M} (left) and $R_{\text{continuum}}$ (right) on the Borel mass. Solid, dashed and dotted curves correspond to the threshold $s_0 = 2.56 \text{ GeV}^2$, 2.66 GeV^2 , 2.46 GeV^2 , respectively, while all the other input parameters are fixed at their central values.

- To reduce the systematic uncertainty induced by the parton-hadron duality approximation, the continuum contributions $R_{\text{continuum}}$ to the correlation functions, displayed in Eq. (44), need to be reasonably controlled, i.e., kept below 40%.
- The sum rule predictions should be stable with respect to variations of the Borel mass parameter ω_M . More concretely, we impose the following condition on the logarithmic derivative of the form factor:

$$R_{\omega_M} \equiv \frac{\partial \ln \xi_\Lambda}{\partial \ln \omega_M} \leq 40\%. \quad (74)$$

We show the dependencies of R_{ω_M} and $R_{\text{continuum}}$ on the sum rule parameter M^2 in Fig. 8. The solid, dashed, and dotted curves correspond to the threshold values $s_0 = 2.56 \text{ GeV}^2$, 2.66 GeV^2 , and 2.46 GeV^2 , respectively, while all other input parameters are fixed at their central values. The flatness of the curves demonstrates that our results exhibit a remarkably weak dependence on the Borel mass parameter. Finally, the allowed ranges of the Borel parameter and the effective duality threshold are determined to be

$$M^2 \equiv n \cdot p \omega_M = (1.6 \pm 0.4) \text{ GeV}^2, \quad s_0 \equiv n \cdot p \omega_s = (2.56 \pm 0.10) \text{ GeV}^2, \quad (75)$$

where the obtained interval for s_0 is in agreement with the values adopted in Refs. [14, 15, 44].

We observe a significant discrepancy in the behavior of R_{ω_M} between our study and the $B \rightarrow \pi$ process. In the $B \rightarrow \pi$ scenario, the leading-order spectral function is given by $\phi_B^-(\omega', \mu)$. As depicted in Fig. 7, its behavior at small ω' differs markedly from that of $\phi_{4,\text{eff}}^{\text{LO}}(\omega', \mu, \nu)$. Moreover, as illustrated in Eq. (52), the mass of the final-state hadron appears in the exponential term. Given that the pion mass is substantially smaller than that of the Λ baryon, this discrepancy in the small- ω' regime contributes to the observed differences. The dependence of R_{ω_M} on M^2 in baryon decay is negligible. In sharp contrast, R_{ω_M} exhibits a much stronger M^2 dependence in the $B \rightarrow \pi$ process.

In order to improve the convergence of the perturbative expansion, we need to resum the large logarithms to all orders in the perturbative matching coefficients by solving the RG evolution equations. However, following the argument of Ref. [34], where it is noted that the characteristic scale of the jet function μ_{hc} is comparable to the hadronic scale μ_0 entering the initial condition of the Λ_b -baryon DA, we will not resum the small logarithms of μ_{hc}/μ_0 arising from the RG running of the hadronic wave function when the factorization scale is chosen to be a hard-collinear scale of order $\sqrt{n \cdot p \Lambda_{\text{QCD}}}$. Furthermore, the normalization parameter $f_{\Lambda_b}^{(2)}(\mu)$ will be taken directly from the HQET sum rule calculation; thus, no RG evolution of $f_{\Lambda_b}^{(2)}(\mu)$ is required [15].

The coupling $f_{\Lambda_b}^{(2)}(\mu_0)$ will be taken from the NLO HQET sum rule calculation, as given in Ref. [45]:

$$f_{\Lambda_b}^{(2)}(1 \text{ GeV}) = (3.0 \pm 0.5) \times 10^{-2} \text{ GeV}^3. \quad (76)$$

To reduce the theoretical uncertainty induced by the Borel mass parameter ω_M , we employ the two-point QCD sum rules for the normalization parameter $f_\Lambda(\nu)$ [46]:

$$f_\Lambda^2 e^{-m_\Lambda^2/M^2} = \frac{1}{640 \pi^4} \int_{m_s^2}^{s_0} ds e^{-s/M^2} s \left(1 - \frac{m_s^2}{s}\right)^5$$

$$-\frac{1}{192\pi^2} \left\langle \frac{\alpha_s}{\pi} GG \right\rangle \int_{m_s^2}^{s_0} ds e^{-s/M^2} \frac{m_s^2}{s^2} \left(1 - \frac{m_s^2}{s}\right) \left(1 - \frac{2m_s^2}{s}\right), \quad (77)$$

evaluated at tree level. For the numerical analysis, we use the gluon condensate density $\langle \alpha_s/\pi GG \rangle = (1.2_{-1.2}^{+0.6}) \times 10^{-2} \text{ GeV}^4$.

For the resummation of large logarithms in the hard functions, we solve the RG equation for the coefficients of the A-type currents, given in Eq. (46). The solution reads [47]

$$C_i^A(n \cdot p, \mu) = \left(\frac{n \cdot p}{\mu_h}\right)^{a(\mu_h, \mu)} \exp \left[S(\mu_h, \mu) + \frac{5C_F}{2\beta_0} \ln r_1 \right] C_i^A(n \cdot p, \mu_h), \quad (78)$$

with [48]

$$\begin{aligned} S(\mu_h, \mu) &= \frac{\Gamma_0}{4\beta_0^2} \left[\frac{4\pi}{\alpha_s(\mu_h)} \left(1 - \frac{1}{r_1} - \ln r_1\right) + \frac{\beta_1}{2\beta_0} \ln^2 r_1 \right. \\ &\quad \left. - \left(\frac{\Gamma_1}{\Gamma_0} - \frac{\beta_1}{\beta_0}\right) (r_1 - 1 - \ln r_1) \right], \\ a(\mu_h, \mu) &= -\frac{\Gamma_0}{2\beta_0} \ln r_1, \end{aligned} \quad (79)$$

where $r_1 = \alpha_s(\mu)/\alpha_s(\mu_h) \geq 1$. For the relevant coefficients entering the cusp anomalous dimension and the β function, we take $n_f = 4$.

We now turn to the discussion of the choices for the renormalization and factorization scales entering the LL sum rules. The renormalization scale ν of the baryonic current and the factorization scale μ will be varied within the interval $1 \text{ GeV} \leq \mu, \nu \leq 2 \text{ GeV}$ around the default value $\mu = \nu = 1.5 \text{ GeV}$. The hard scale μ_h appearing in the hard matching coefficients will be set to $\mu_h = m_b$, with variations in the range $[m_b/2, 2m_b]$. For the $\Lambda_b \rightarrow \Lambda \gamma$ process, due to the specific logarithmic structure of the hard coefficient in Eq. (121), the hard scale will instead be taken as $\mu_h = m_b^{\text{pole}}$, varied within the range $[m_b, M_{\Lambda_b}]$. In addition, we adopt the $\overline{\text{MS}}$ bottom-quark mass $\overline{m}_b(\overline{m}_b) = 4.183 \pm 0.007 \text{ GeV}$ and the strange-quark mass $\overline{m}_s(\overline{m}_s) = 0.0935 \pm 0.0008 \text{ GeV}$ [49]. The pole masses of the b - and c -quarks are deduced from the PS mass [50, 51].

4.2 Predictions for the $\Lambda_b \rightarrow \Lambda$ effective form factors

To illustrate key numerical features of the LCSR predictions, we present the dependencies of $\xi_\Lambda(q^2 = 0)$ on the sum rule parameters M^2 and s_0 , as well as on the factorization scale μ , in Fig. 9. It is evident that the sum rule for $\xi_\Lambda(q^2 = 0)$ exhibits exceptionally mild dependence on the Borel mass parameter, owing to a strong cancellation of systematic uncertainties between the LCSR prediction for $\xi_\Lambda(q^2 = 0)$ and the QCD sum rule for the coupling f_Λ . Also the three different choices of s_0 introduce only a negligible difference to the form factor. In our case, the NLO sum rules show sensitivity to the factorization scale μ , since SCET form factors do not involve hard matching coefficients as in the QCD LCSR framework.

We now turn to investigate the Λ -baryon energy dependence of the form factor $\xi_\Lambda(n \cdot p)$ using the sum rules at LO and NLO accuracy. This study is of particular conceptual interest since the soft-overlap contributions and the hard-spectator scattering effects in heavy-to-light

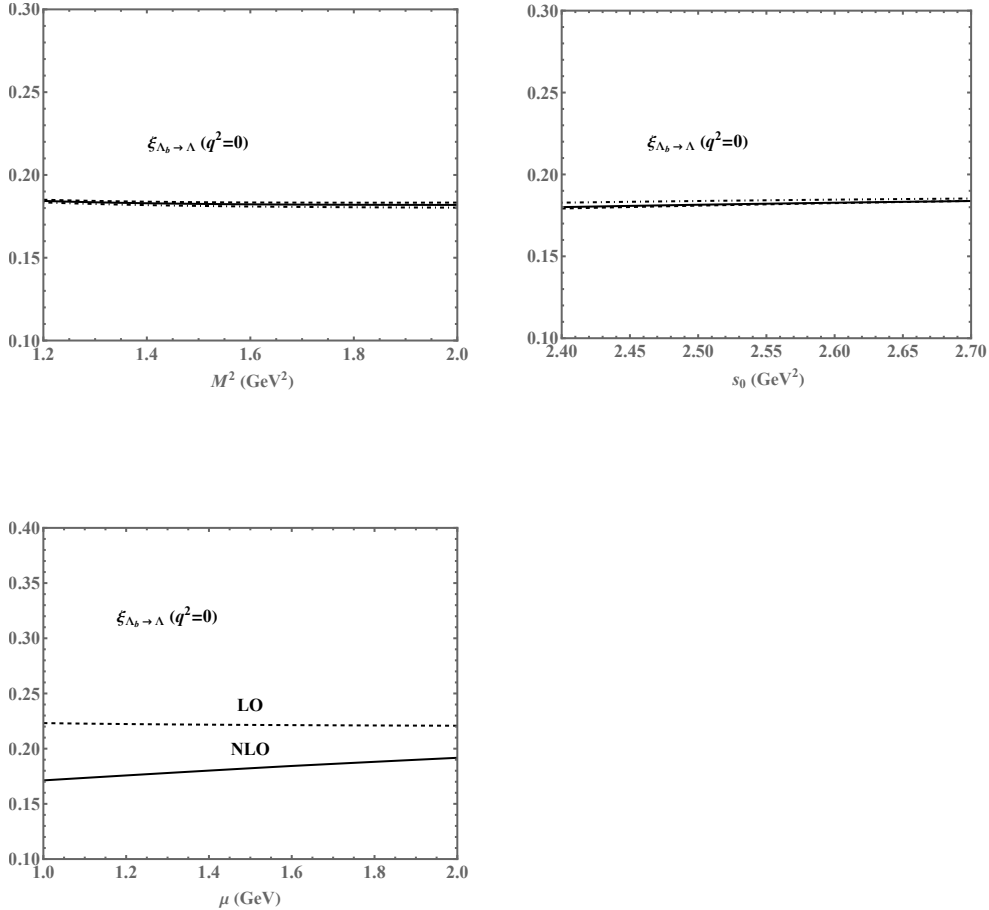


Figure 9: Dependence of $\xi_\Lambda(q^2 = 0)$ on the Borel parameter (top left), on the threshold parameter (top right) and on the factorization scale (bottom left). Solid, dashed and dotted-dashed curves are obtained from the sum rules with $s_0 = 2.56 \text{ GeV}^2$, 2.66 GeV^2 , 2.46 GeV^2 (top left) and $M^2 = 1.6 \text{ GeV}^2$, 2.0 GeV^2 , 1.2 GeV^2 (top right), respectively, while all the other input parameters are fixed at their central values. The curves labelled by “LO” and “NLO” (bottom) correspond to the sum rule predictions at LO and NLO accuracy.

baryonic form factors exhibit different scalings with respect to $1/E_\Lambda$ at large hadronic recoil. To this end, we introduce the ratio originally proposed in Ref. [30]:

$$R_1(E_\Lambda) = \frac{\xi_\Lambda(n \cdot p)}{\xi_\Lambda(m_{\Lambda_b})}. \quad (80)$$

As shown in Fig. 10, the predicted energy dependence of ξ_Λ from the LO and NLO sum rules displays a scaling behavior between $1/E_\Lambda^2$ and $1/E_\Lambda^3$ for the default choices of theory input parameters.

As discussed in Sec. 3.1.3, the leading-power contribution to ξ_Λ is $\mathcal{O}(\alpha_s^2)$, with the numerical estimate [37]

$$\xi_\Lambda^{\text{LP}}(q^2 = 0) = -0.012_{-0.023}^{+0.009}. \quad (81)$$

The soft contributions calculated in this work are

$$\xi_\Lambda^{\text{LO}}(q^2 = 0) = 0.222_{-0.058}^{+0.057}, \quad \xi_\Lambda^{\text{NLO}}(q^2 = 0) = 0.182_{-0.041}^{+0.050}. \quad (82)$$

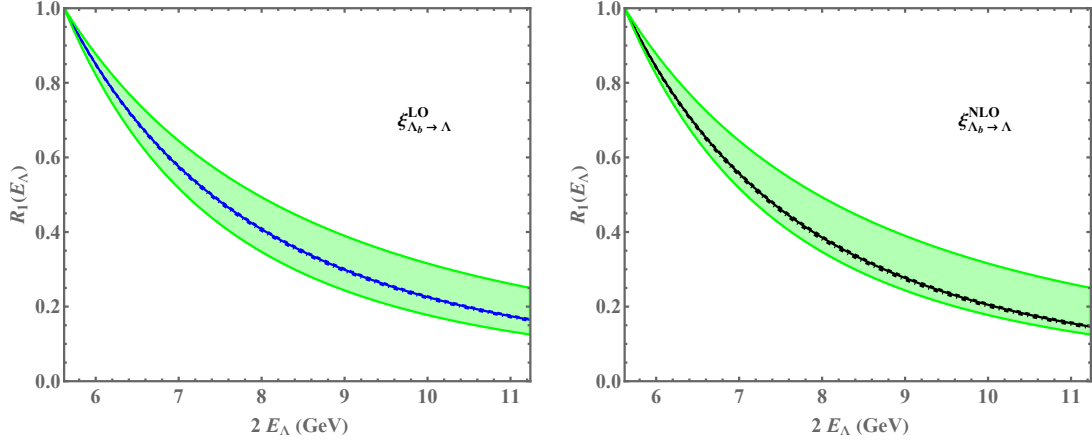


Figure 10: Dependence of the ratio $R_1(E_\Lambda)$ on the Λ -baryon energy E_Λ . The blue (left panel) and the black (right panel) curves are obtained from the LO and NLO sum rule predictions, respectively. The two green curves refer to a pure $1/E_\Lambda^2$ and a pure $1/E_\Lambda^3$ dependence.

The dominant theoretical uncertainty for the form factor at $q^2 = 0$ computed from the SCET LCSR arises from the variation of the parameter ω_0 entering the Λ_b -baryon DA $\phi_4(\omega, \mu_0)$. Comparing Eqs. (81) and (82), we observe that the A-type form factor is numerically dominated by soft contributions, despite being formally power-suppressed. This observation is consistent with the conclusions of Ref. [37].

To estimate the non-factorizable contributions, we also calculate the C-type form factor $\Delta\xi_\Lambda^C(u, n \cdot p)$. To preserve quark-hadron duality, we restrict our analysis to q^2 values exceeding the masses of narrow vector resonances like the ρ and ω mesons [21]. Accordingly, we evaluate our LCSRs at the following q^2 points: $q^2 = \{2, 4, 6\} \text{ GeV}^2$,

$$\begin{aligned}
 10^4 \cdot \int du \Delta\xi_\Lambda^C(u, q^2 = 2 \text{ GeV}^2) &= -(1.06 \pm 0.19) - i(2.49 \pm 0.77), \\
 10^4 \cdot \int du \Delta\xi_\Lambda^C(u, q^2 = 4 \text{ GeV}^2) &= (0.45 \pm 0.40) - i(2.29 \pm 0.54), \\
 10^4 \cdot \int du \Delta\xi_\Lambda^C(u, q^2 = 6 \text{ GeV}^2) &= (1.09 \pm 0.42) - i(1.58 \pm 0.28).
 \end{aligned}
 \tag{83}$$

The non-factorizable contributions to the $\Lambda_b \rightarrow \Lambda \ell^+ \ell^-$ and $\Lambda_b \rightarrow \Lambda \gamma$ decay amplitudes can be expressed as shifts in the hard functions C_1^A and C_γ^A , as given in Eq. (73). For $\Lambda_b \rightarrow \Lambda \gamma$ decay, we find

$$\frac{|\Delta C_\gamma^A|}{|C_\gamma^A|} < 2\%
 \tag{84}$$

at the scale $\mu = m_b^{\text{pole}}$. In the case of $\Lambda_b \rightarrow \Lambda \ell^+ \ell^-$ decay, the ratio $|\Delta C_1^A|/|C_1^A|$ is typically $\mathcal{O}(1\%)$ across most of the region $1 \text{ GeV}^2 < q^2 < 7 \text{ GeV}^2$. However, a notable peak appears around $q^2 \sim 3.2 \text{ GeV}^2$, where

$$\frac{|\Delta C_1^A(q^2 \sim 3.2 \text{ GeV}^2)|}{|C_1^A(q^2 \sim 3.2 \text{ GeV}^2)|} \sim 50\%.
 \tag{85}$$

This peak arises because both the operators \mathcal{Q}_7 and \mathcal{Q}_9 contribute to C_1^A , and their effects largely cancel each other near $q^2 = 3.2 \text{ GeV}^2$. As a result, at the amplitude level, the operator \mathcal{Q}_{10} dominates in this region. In full QCD, operators \mathcal{Q}_7 and \mathcal{Q}_9 will contribute to different form factors, and the non-factorizable effects can be interpreted as a shift in C_9 . As demonstrated in Ref. [21], the relative shift $|\Delta C_{9,\perp}|/|C_9|$ is only $\mathcal{O}(1\%)$. These results indicate that the non-factorizable contributions to the branching ratios remain relatively small. Moreover, the one-loop matching of C-type operators from QCD to SCET_I is incomplete, and the renormalization group equations for these operators are not yet available. Therefore, we neglect the non-factorizable contributions in our phenomenological analysis and defer their detailed study to future work.

5 Phenomenological applications

In this section, we explore the phenomenological applications of the calculated ξ_Λ form factor, which serves as a fundamental ingredient in the theoretical description of the electroweak penguin-induced $\Lambda_b \rightarrow \Lambda \ell^+ \ell^-$ and $\Lambda_b \rightarrow \Lambda \gamma$ decays. As discussed in Sec. 4.2, we restrict ourselves to the factorizable contributions to the decay amplitudes.

The double differential decay distribution of $\Lambda_b \rightarrow \Lambda \ell^+ \ell^-$, in terms of the momentum transfer squared q^2 and the angle θ between the negatively charged lepton and the Λ baryon in the rest frame of the lepton pair, is derived in Appendix B:

$$\frac{d\Gamma(\Lambda_b \rightarrow \Lambda \ell^+ \ell^-)}{dq^2 d\cos\theta} = \mathcal{N} [F_T(q^2) (1 + \cos^2\theta) + 2F_A(q^2) \cos\theta + 2F_L(q^2) (1 - \cos^2\theta)]. \quad (86)$$

Evaluating the helicity amplitudes with the form factor computed from the LL LCSR obtained above yields the differential branching fraction of $\Lambda_b \rightarrow \Lambda \ell^+ \ell^-$ as a function of q^2 , shown in Fig. 11. The theory predictions are also compared with experimental measurements from CDF [52] and LHCb [53]. The LHCb data are systematically lower than the theory predictions at large recoil, while the sizable uncertainties in the CDF measurements, combined with the large theoretical uncertainties at high q^2 , prevent drawing a definite conclusion.

Following Ref. [53], we further consider the forward-backward asymmetry and the longitudinal polarization fraction of the di-lepton system:

$$A_{\text{FB}}(q^2) = \frac{\int_{-1}^0 d\cos\theta \frac{d\Gamma(\Lambda_b \rightarrow \Lambda \ell^+ \ell^-)}{dq^2 d\cos\theta} - \int_0^1 d\cos\theta \frac{d\Gamma(\Lambda_b \rightarrow \Lambda \ell^+ \ell^-)}{dq^2 d\cos\theta}}{\frac{d\Gamma(\Lambda_b \rightarrow \Lambda \ell^+ \ell^-)}{dq^2}},$$

$$f_L(q^2) = \frac{F_L(q^2)}{F_L(q^2) + F_T(q^2)}, \quad (87)$$

where the definition of $A_{\text{FB}}(q^2)$ differs from Refs. [14, 15] due to a distinct convention for the angle θ . We also plot the q^2 dependence of the differential forward-backward asymmetry and the longitudinal polarization fraction in Fig. 11. It is apparent that the theoretical uncertainties for these two observables are much smaller than those for the branching ratios, owing to partial cancellation of uncertainties in the ratios defined in Eq. (87). However, as seen in Fig. 11, the experimental uncertainties for these observables remain quite large. We

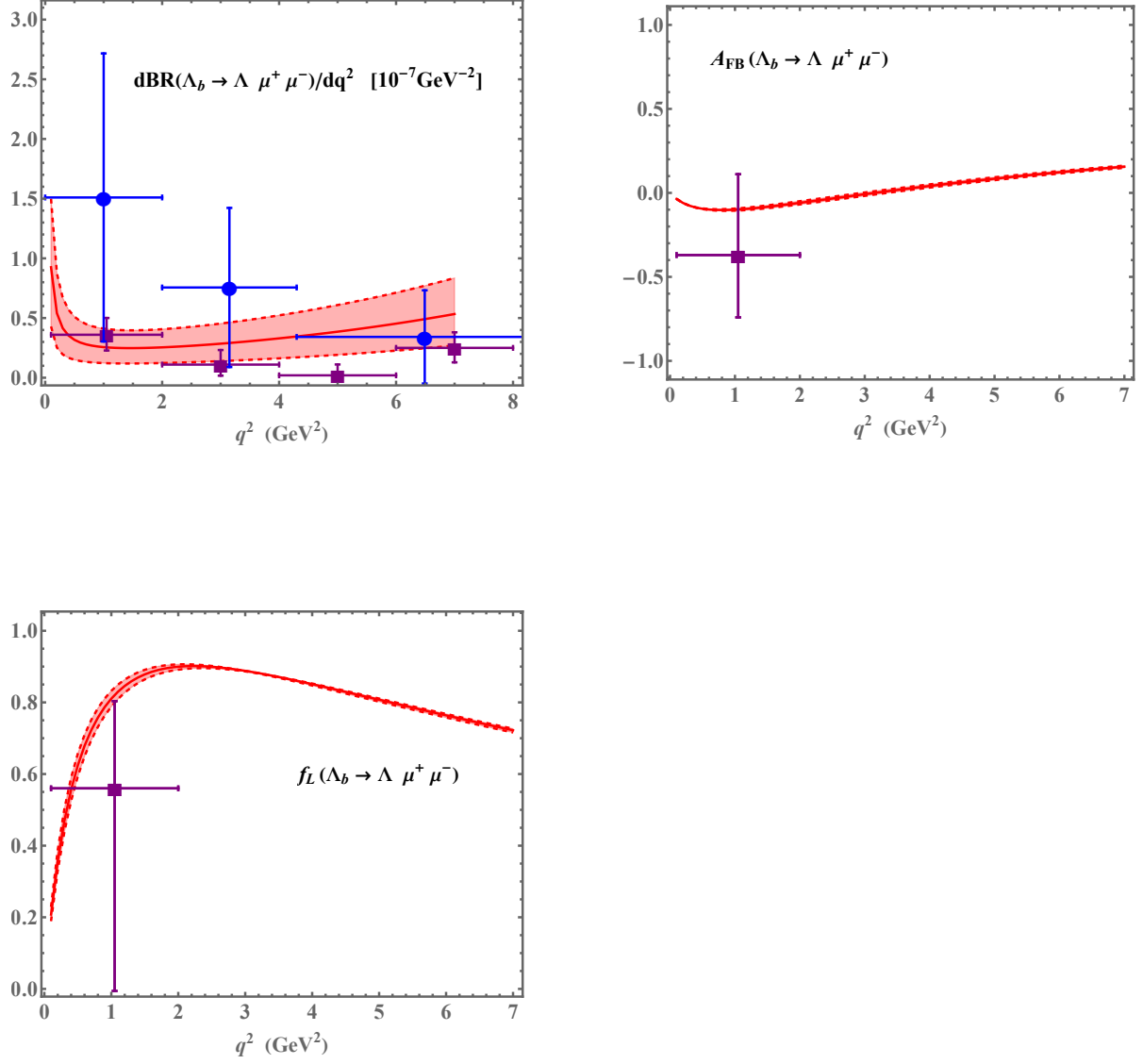


Figure 11: The differential branching fraction, the leptonic forward-backward asymmetry and the longitudinal polarization fraction of the di-lepton system for $\Lambda_b \rightarrow \Lambda \ell^+ \ell^-$ as functions of q^2 in the factorization limit. The solid (pink) curve corresponds to the LL sum rule predictions with the shaded region (pink) indicating the theory uncertainties from form factor. The experimental data bins are taken from LHCb [53] (purple squares) and CDF [52] (blue full circles).

expect future data to shed more light on the rich phenomenology encoded in the angular distributions of $\Lambda_b \rightarrow \Lambda \ell^+ \ell^-$, with an emphasis on optimized physics observables that are especially sensitive for new physics searches.

With the soft form factor ξ_Λ at $q^2 = 0$ in hand, we further analyze the $\Lambda_b \rightarrow \Lambda \gamma$ decay in Appendix B. Employing Eq. (123), we obtain

$$\mathcal{B}(\Lambda_b \rightarrow \Lambda \gamma) = (1.22_{-0.67}^{+0.66}) \times 10^{-5}, \quad (88)$$

while the experimental value, reported in [49], is $(7.1 \pm 1.7) \times 10^{-6}$. Our analysis shows that the central theoretical prediction is slightly larger than the experimental measurement. However, it is important to emphasize that the experimental value lies within the theoretical uncertainty band, and both theoretical and experimental uncertainties remain sizable. Considering both experimental and theoretical uncertainties, our prediction is consistent with the current data. In our future work, reducing theoretical errors will be one of our primary tasks. On one hand, within the framework of LCSRs, we can minimize the input parameters such as that in the Λ_b distribution amplitudes. On the other hand, we can conduct joint fits by combining lattice simulation results of transition form factors and our calculations.

6 Conclusions

In this work, we study the $\Lambda_b \rightarrow \Lambda \ell^+ \ell^-$ and $\Lambda_b \rightarrow \Lambda \gamma$ decays using light-cone sum rules within the soft-collinear effective theory framework. To obtain the decay amplitudes, we parameterize the matrix elements of SCET_I operators in terms of effective form factors. Employing light-cone sum rules, we perform the perturbative matching from SCET_I to SCET_{II} to determine the hard-collinear functions in the SCET factorization framework.

For the A-type effective form factor ξ_Λ , we obtain the soft form factor up to NLO accuracy, and the resulting jet function matches that derived using LCSR combined with the method of regions. The leading-power contribution of the form factor is α_s^2 suppressed compared to the soft form factor. The form factor $\Delta \xi_\Lambda^B$ represents a non-local form factor associated with hard-scattering corrections mediated by hard-collinear gluon exchange. This form factor vanishes at leading power in the relevant correlation functions, indicating that the hard-scattering corrections are power-suppressed relative to the “soft” contribution. This behavior is distinct from that observed in B -meson decays. The C-type form factors $\Delta_k \xi_\Lambda^C$ also represent non-local form factors corresponding to non-factorizable contributions. To calculate the hard coefficients of the C-type SCET_I operators, we consider not only the weak annihilation contribution but also quark-loop and chromomagnetic contributions. We then carry out the SCET_I \rightarrow SCET_{II} matching of the γ^* -to- Λ_b correlation functions to derive these form factors, and find $\Delta_1 \xi_\Lambda^C = \Delta_2 \xi_\Lambda^C = 0$ and $\Delta_3 \xi_\Lambda^C = -\Delta_4 \xi_\Lambda^C$. At the amplitude level, we find that the C-type non-factorizable contributions are numerically suppressed, indicating that the Λ_b decay processes are dominated by the “soft” contributions.

We compute the q^2 -dependent differential branching fractions in the factorization limit, the forward-backward asymmetries, and the dilepton longitudinal polarization fractions for

$\Lambda_b \rightarrow \Lambda \ell^+ \ell^-$ decays, as well as the branching fractions for $\Lambda_b \rightarrow \Lambda \gamma$ decays. The theoretical predictions for the branching fractions carry substantial uncertainties, dominated by the poorly constrained Λ_b LCDAs. This situation underscores the urgent need for improved determinations of these non-perturbative parameters in future investigations (see recent developments in Refs. [54, 55]). In striking contrast, the forward-backward asymmetry and dilepton longitudinal polarization fraction exhibit remarkably small theoretical uncertainties, benefiting from significant cancellation of parametric errors in their ratio definitions.

In summary, this theoretical investigation establishes a robust framework for analyzing strong interaction effects in exclusive Λ_b -baryon decays within the SCET formalism. Our results not only provide crucial insights into the factorization properties and power counting of these processes, but also lay the groundwork for future precision studies. Given the remarkable progress in experimental capabilities for beauty baryon decays at LHCb and future colliders, we anticipate that this work will inspire several important extensions, including calculations of higher-order corrections, explorations of additional decay channels, and more comprehensive analyses incorporating improved determinations of baryon distribution amplitudes.

Acknowledgements

We thank Jian-Peng Wang for his help to the derivation of angular distributions. This work is supported in part by the National Key Research and Development Program of China (2023YFA1606000), Natural Science Foundation of China under grant No.12175218, 12275277, 12305099 and 12435004 and the Natural Science Foundation of Shandong Province under the Grant No. ZR2024MA076.

A Light-Cone Distribution Amplitudes

The most general non-local matrix elements for Λ_b baryon in coordinate space is [14]:

$$\begin{aligned} & \epsilon_{ijk} \langle 0 | (u_\alpha^i(z_1) d_\beta^j(z_2)) h_v^k(0) | \Lambda_b(v, s) \rangle \\ & \equiv \frac{1}{4} \left\{ f_{\Lambda_b}^{(1)} \left[\tilde{M}^{(1)}(v, z_1, z_2) \gamma_5 C^T \right]_{\beta\alpha} + f_{\Lambda_b}^{(2)} \left[\tilde{M}^{(2)}(v, z_1, z_2) \gamma_5 C^T \right]_{\beta\alpha} \right\} u_{\Lambda_b}(v, s), \end{aligned} \quad (89)$$

with a part that contains an odd number of Dirac matrices $\tilde{M}^{(2)}(v, z_1, z_2)$, and a part that contains an even number of Dirac matrices $\tilde{M}^{(1)}(v, z_1, z_2)$.

The standard LCDAs can be obtained by expanding the above expression around the limit $z_1^2 = z_2^2 = z_1 \cdot z_2 = 0$ (correspond to multiple expand in SCET). As shown in Ref. [42], in this limit, $\bar{n} \cdot z_i \ll z_i^\perp \ll n \cdot z_i$,

$$\begin{aligned} \tilde{M}^{(2)}(v, z_1, z_2) & \longrightarrow \frac{\not{n}}{2} \tilde{\phi}_2(\tau_1, \tau_2) + \frac{\not{n}}{2} \left(\tilde{\phi}_2(\tau_1, \tau_2) + \tilde{\phi}_{42}^{(i)}(\tau_1, \tau_2) + \tilde{\phi}_{42}^{(ii)}(\tau_1, \tau_2) \right) \\ & \quad + \frac{\tilde{\phi}_{42}^{(i)}(\tau_1, \tau_2)}{2\tau_1} \not{\epsilon}_1^\perp + \frac{\tilde{\phi}_{42}^{(ii)}(\tau_1, \tau_2)}{2\tau_2} \not{\epsilon}_2^\perp \end{aligned}$$

$$+ \tilde{\phi}_X(\tau_1, \tau_2) \left(\frac{\not{\epsilon}_1^\perp}{2\tau_1} - \frac{\not{\epsilon}_2^\perp}{2\tau_2} \right) \left(\frac{\not{\eta}\not{\eta}}{4} - \frac{\not{\eta}\not{\eta}}{4} \right) + \mathcal{O}(z_{i\perp}^2, \bar{n} \cdot z_i), \quad (90)$$

where we denote with $\tau_i = \frac{n \cdot z_i}{2}$ the Fourier-conjugate variables to the momentum components $\omega_i = \bar{n} \cdot k_i$ of the associated light-quark states in the heavy baryon. After Fourier transformation, the general momentum-space representation for Eq. (90) including the first-order terms off the light-cone (in D dimensions) becomes

$$\begin{aligned} M^{(2)}(\omega_1, \omega_2) &= \frac{\not{\eta}}{2} \phi_2(\omega_1, \omega_2) + \frac{\not{\eta}}{2} \phi_4(\omega_1, \omega_2) \\ &- \frac{1}{D-2} \gamma_\mu^\perp \int_0^{\omega_1} d\eta_1 \left(\phi_{42}^{(i)}(\eta_1, \omega_2) - \phi_X(\eta_1, \omega_2) \right) \frac{\not{\eta}\not{\eta}}{4} \frac{\partial}{\partial k_{1\mu}^\perp} \\ &- \frac{1}{D-2} \gamma_\mu^\perp \int_0^{\omega_1} d\eta_1 \left(\phi_{42}^{(i)}(\eta_1, \omega_2) + \phi_X(\eta_1, \omega_2) \right) \frac{\not{\eta}\not{\eta}}{4} \frac{\partial}{\partial k_{1\mu}^\perp} \\ &- \frac{1}{D-2} \gamma_\mu^\perp \int_0^{\omega_2} d\eta_2 \left(\phi_{42}^{(ii)}(\omega_1, \eta_2) - \phi_X(\omega_1, \eta_2) \right) \frac{\not{\eta}\not{\eta}}{4} \frac{\partial}{\partial k_{2\mu}^\perp} \\ &- \frac{1}{D-2} \gamma_\mu^\perp \int_0^{\omega_2} d\eta_2 \left(\phi_{42}^{(ii)}(\omega_1, \eta_2) + \phi_X(\omega_1, \eta_2) \right) \frac{\not{\eta}\not{\eta}}{4} \frac{\partial}{\partial k_{2\mu}^\perp}. \end{aligned} \quad (91)$$

In the Wandzura-Wilczek approximation,

$$\begin{aligned} \int_0^{\omega_1} d\eta_1 \left(\phi_{42}^{(i)}(\eta_1, \omega_2) + \phi_X(\eta_1, \omega_2) \right) &= \omega_1 \phi_4(\omega_1, \omega_2), \\ \int_0^{\omega_2} d\eta_2 \left(\phi_{42}^{(ii)}(\omega_1, \eta_2) + \phi_X(\omega_1, \eta_2) \right) &= \omega_2 \phi_4(\omega_1, \omega_2). \end{aligned} \quad (92)$$

With the most general form of the momentum-space projectors, we can write

$$\phi_4(\omega_1, \omega_2) = \int_{\omega_1}^{\infty} dx_1 \int_{\omega_2}^{\infty} dx_2 (x_1 - \omega_1)(x_2 - \omega_2) \psi_v(x_1, x_2). \quad (93)$$

In the simplest case, we could model the wave functions by assuming an exponential dependence of ψ_v on $(x_1 + x_2)$ with a single hadronic parameter ω_0 measuring the average energy of the light quarks,

$$\psi_v(x_1, x_2) \rightarrow \frac{\exp\left(-\frac{x_1+x_2}{\omega_0}\right)}{\omega_0^6}. \quad (94)$$

This ansatz yields the following exponential model,

$$\phi_4(\omega_1, \omega_2) \rightarrow \frac{1}{\omega_0^2} e^{-(\omega_1+\omega_2)/\omega_0}. \quad (95)$$

However, when we calculate the non-factorizable contributions in Fig. 6, we rather have to consider the expansion for the situation $n \cdot z_1 \ll z_1^\perp \ll \bar{n} \cdot z_1$ and $\bar{n} \cdot z_2 \ll z_2^\perp \ll n \cdot z_2$, such that $t_1 \approx \bar{\tau}_1 = \frac{\bar{n} \cdot z_1}{2}$, $t_2 \approx \tau_2 = \frac{n \cdot z_2}{2}$, and $z_1 \cdot z_2 \approx 2\bar{\tau}_1\tau_2$. For completeness, we adopt the methodology established in Refs. [21, 42] to derive the momentum projectors in this case. The momentum-space projector for matrix $\tilde{M}^{(1)}$ takes the form:

$$M^{(1)}(\bar{\omega}_1, \omega_2) = \frac{\not{\eta}\not{\eta}}{4} \left(\chi_3^{(0)}(\bar{\omega}_1, \omega_2) - \chi_Y(\bar{\omega}_1, \omega_2) \right)$$

$$\begin{aligned}
& + \frac{\not{n}\not{n}}{4} \left(\chi_3^{(0)}(\bar{\omega}_1, \omega_2) + \chi_Y(\bar{\omega}_1, \omega_2) + \chi_3^{(i)}(\bar{\omega}_1, \omega_2) + \chi_3^{(ii)}(\bar{\omega}_1, \omega_2) \right) \\
& + \frac{1}{2} \gamma_\rho^\perp \bar{\chi}_3^{(i)}(\bar{\omega}_1, \omega_2) \frac{\not{n}}{2} \frac{\partial}{\partial k_{1\rho}^\perp} \\
& + \frac{1}{2} \gamma_\rho^\perp \left(\bar{\chi}_3^{(i)}(\bar{\omega}_1, \omega_2) + 2\bar{\chi}_Y(\bar{\omega}_1, \omega_2) \right) \frac{\not{n}}{2} \frac{\partial}{\partial k_{1\rho}^\perp} \\
& - \frac{1}{2} \gamma_\rho^\perp \hat{\chi}_3^{(ii)}(\bar{\omega}_1, \omega_2) \frac{\not{n}}{2} \frac{\partial}{\partial k_{2\rho}^\perp} \\
& - \frac{1}{2} \gamma_\rho^\perp \left(\hat{\chi}_3^{(ii)}(\bar{\omega}_1, \omega_2) + 2\hat{\chi}_Y(\bar{\omega}_1, \omega_2) \right) \frac{\not{n}}{2} \frac{\partial}{\partial k_{2\rho}^\perp}. \tag{96}
\end{aligned}$$

Here, the derivatives operate on a hard-scattering kernel that has been expanded in transverse momenta, where we define $\bar{\omega}_1 = n \cdot k_1$ and $\omega_2 = \bar{n} \cdot k_2$. Using the simplified exponential model for baryon wave functions, we derive the following expressions for the relevant linear combinations appearing in the momentum-space projector:

$$\chi_3^{(0)}(\bar{\omega}_1, \omega_2) - \chi_Y(\bar{\omega}_1, \omega_2) = \frac{\bar{\omega}_1 \omega_2}{\omega_0^4} e^{-(\bar{\omega}_1 + \omega_2)/\omega_0}, \tag{97}$$

$$\chi_3^{(0)}(\bar{\omega}_1, \omega_2) + \chi_Y(\bar{\omega}_1, \omega_2) + \chi_3^{(i)}(\bar{\omega}_1, \omega_2) + \chi_3^{(ii)}(\bar{\omega}_1, \omega_2) = \frac{1}{\omega_0^2} e^{-(\bar{\omega}_1 + \omega_2)/\omega_0}, \tag{98}$$

$$\bar{\chi}_3^{(i)}(\bar{\omega}_1, \omega_2) = \frac{\bar{\omega}_1 \omega_2}{\omega_0^3} e^{-(\bar{\omega}_1 + \omega_2)/\omega_0}, \tag{99}$$

$$\bar{\chi}_3^{(i)}(\bar{\omega}_1, \omega_2) + 2\bar{\chi}_Y(\bar{\omega}_1, \omega_2) = \frac{\bar{\omega}_1}{\omega_0^2} e^{-(\bar{\omega}_1 + \omega_2)/\omega_0}, \tag{100}$$

$$\hat{\chi}_3^{(ii)}(\bar{\omega}_1, \omega_2) = \frac{\bar{\omega}_1 \omega_2}{\omega_0^3} e^{-(\bar{\omega}_1 + \omega_2)/\omega_0}, \tag{101}$$

$$\hat{\chi}_3^{(ii)}(\bar{\omega}_1, \omega_2) + 2\hat{\chi}_Y(\bar{\omega}_1, \omega_2) = \frac{\omega_2}{\omega_0^2} e^{-(\bar{\omega}_1 + \omega_2)/\omega_0}. \tag{102}$$

We should note that the arguments $\bar{\omega}_1$ and ω_2 in the generalized distribution amplitude are generally not positive definite. This is because the definition of generalized distribution amplitudes requires introducing two Wilson lines with different light-cone directions. The renormalization group evolution kernel of these amplitudes contains a mixing pattern that couples positive and negative supports, thereby extending the support region to the entire real axis [56, 57].

The matrix $\tilde{M}^{(2)}$, whose explicit form was obtained in Ref. [21], follows the same treatment:

$$\begin{aligned}
M^{(2)}(\bar{\omega}_1, \omega_2) & = \frac{\not{n}}{2} \left(\chi_2(\bar{\omega}_1, \omega_2) + \chi_{42}^{(i)}(\bar{\omega}_1, \omega_2) \right) \\
& + \frac{\not{n}}{2} \left(\chi_2(\bar{\omega}_1, \omega_2) + \chi_{42}^{(ii)}(\bar{\omega}_1, \omega_2) \right) \\
& - \frac{1}{2} \gamma_\rho^\perp \left(\bar{\chi}_{42}^{(i)}(\bar{\omega}_1, \omega_2) - \bar{\chi}_X(\bar{\omega}_1, \omega_2) \right) \frac{\not{n}\not{n}}{4} \frac{\partial}{\partial k_{1\rho}^\perp} \\
& - \frac{1}{2} \gamma_\rho^\perp \left(\bar{\chi}_{42}^{(i)}(\bar{\omega}_1, \omega_2) + \bar{\chi}_X(\bar{\omega}_1, \omega_2) \right) \frac{\not{n}\not{n}}{4} \frac{\partial}{\partial k_{1\rho}^\perp} \\
& - \frac{1}{2} \gamma_\rho^\perp \left(\hat{\chi}_{42}^{(ii)}(\bar{\omega}_1, \omega_2) + \hat{\chi}_X(\bar{\omega}_1, \omega_2) \right) \frac{\not{n}\not{n}}{4} \frac{\partial}{\partial k_{2\rho}^\perp}
\end{aligned}$$

$$-\frac{1}{2} \gamma_\rho^\perp \left(\hat{\chi}_{42}^{(ii)}(\bar{\omega}_1, \omega_2) - \hat{\chi}_X(\bar{\omega}_1, \omega_2) \right) \frac{\not{\eta} \not{\eta}}{4} \frac{\partial}{\partial k_{2\rho}^\perp}, \quad (103)$$

and

$$\chi_2(\bar{\omega}_1, \omega_2) + \chi_{42}^{(i)}(\bar{\omega}_1, \omega_2) = \frac{\omega_2}{\omega_0^3} e^{-(\bar{\omega}_1 + \omega_2)/\omega_0}, \quad (104)$$

$$\chi_2(\bar{\omega}_1, \omega_2) + \chi_{42}^{(ii)}(\bar{\omega}_1, \omega_2) = \frac{\bar{\omega}_1}{\omega_0^3} e^{-(\bar{\omega}_1 + \omega_2)/\omega_0}, \quad (105)$$

$$\bar{\chi}_{42}^{(i)}(\bar{\omega}_1, \omega_2) - \bar{\chi}_X(\bar{\omega}_1, \omega_2) = \frac{\bar{\omega}_1 \omega_2}{\omega_0^3} e^{-(\bar{\omega}_1 + \omega_2)/\omega_0}, \quad (106)$$

$$\bar{\chi}_{42}^{(ii)}(\bar{\omega}_1, \omega_2) + \bar{\chi}_X(\bar{\omega}_1, \omega_2) = \frac{\bar{\omega}_1}{\omega_0^2} e^{-(\bar{\omega}_1 + \omega_2)/\omega_0}, \quad (107)$$

$$\hat{\chi}_{42}^{(ii)}(\bar{\omega}_1, \omega_2) + \hat{\chi}_X(\bar{\omega}_1, \omega_2) = \frac{\omega_2}{\omega_0^2} e^{-(\bar{\omega}_1 + \omega_2)/\omega_0}, \quad (108)$$

$$\hat{\chi}_{42}^{(ii)}(\bar{\omega}_1, \omega_2) - \hat{\chi}_X(\bar{\omega}_1, \omega_2) = \frac{\bar{\omega}_1 \omega_2}{\omega_0^3} e^{-(\bar{\omega}_1 + \omega_2)/\omega_0}. \quad (109)$$

B Decay distribution in the helicity formalism

In this Appendix, we derive the branching ratios for the decays $\Lambda_b \rightarrow \Lambda \ell^+ \ell^-$ and $\Lambda \gamma$ in terms of the effective form factor $\xi_\Lambda(n \cdot p)$. Following Ref. [58], we derive the $\Lambda_b \rightarrow \Lambda \ell^+ \ell^-$ decay angular distribution in the helicity formalism. Starting from the helicity amplitudes defined in Eq. (23), we can further write it as

$$\mathcal{M}(s, s', s_1, s_2) = -\xi_\Lambda(n \cdot p) \sum_\lambda \eta_\lambda \left[H_V^\lambda(s, s') L_V^\lambda(s_1, s_2) + H_A^\lambda(s, s') L_A^\lambda(s_1, s_2) \right]. \quad (110)$$

Here $\lambda = t, \pm 1, 0$ are the polarization states of the virtual gauge boson that decays into dilepton pair, $\eta_t = 1$ and $\eta_{\pm 1, 0} = -1$. $H_{V(A)}^\lambda$ and $L_{V(A)}^\lambda$ are the hadronic and leptonic helicity amplitudes corresponding the vector(V) and axial-vector(A) lepton currents.

The hadronic helicity amplitudes are the projections of $\Lambda_b \rightarrow \Lambda$ matrix elements on the direction of the polarization of virtual gauge boson,

$$H_V^\lambda(s, s') = \bar{\epsilon}_\mu^*(\lambda) \left[C_1^A(E) \bar{u}_\Lambda(p, s') (1 + \gamma_5) \gamma_\perp^\mu u_{\Lambda_b}(P, s) + C_2^A(E) \bar{u}_\Lambda(p, s') (1 + \gamma_5) u_{\Lambda_b}(P, s) \bar{n}^\mu \right], \quad (111)$$

$$H_A^\lambda(s, s') = \bar{\epsilon}_\mu^*(\lambda) \left[C_3^A(E) \bar{u}_\Lambda(p, s') (1 + \gamma_5) \gamma_\perp^\mu u_{\Lambda_b}(P, s) + C_4^A(E) \bar{u}_\Lambda(p, s') (1 + \gamma_5) u_{\Lambda_b}(P, s) \bar{n}^\mu \right]. \quad (112)$$

Similarly, the leptonic helicity amplitudes are

$$L_V^\lambda = \bar{\epsilon}_\nu(\lambda) \bar{u}(p_1, s_1) \gamma^\nu v(p_2, s_2), \quad (113)$$

$$L_A^\lambda = \bar{\epsilon}_\nu(\lambda) \bar{u}(p_1, s_1) \gamma^\nu \gamma_5 v(p_2, s_2). \quad (114)$$

Here $\bar{\epsilon}_\nu(\lambda)$ denotes the polarization vector of the virtual gauge boson. Our choice for the polarization vectors are the same as Ref. [58]. The spinor matrix elements for different combinations of spin orientations are collected in Appendix D of Ref. [58]. Neglecting the mass of the leptons, the leptonic helicity amplitudes can be found in Eq.(B.3)³ of Ref. [59]. Using these results we can write down the expressions of the helicity amplitudes $\mathcal{M}(s, s', s_1, s_2)$ directly. Finally we get

$$\begin{aligned} \frac{d\Gamma(\Lambda_b \rightarrow \Lambda \ell^+ \ell^-)}{dq^2 d\cos\theta} &= \frac{\lambda}{512 M_{\Lambda_b}^3 \pi^3} \times \frac{1}{2} \sum_s \sum_{s'} \sum_{s_1} \sum_{s_2} |\mathcal{M}(s, s', s_1, s_2)|^2 \\ &= \mathcal{N} [F_T(q^2) (1 + \cos^2\theta) + 2 F_A(q^2) \cos\theta + 2 F_L(q^2) (1 - \cos^2\theta)], \end{aligned} \quad (115)$$

where in the factorization limit the helicity amplitudes can be computed as

$$F_T(q^2) = |\xi_\Lambda(n \cdot p)|^2 \lambda (s_+ + s_-) q^2 (|C_1^A|^2 + |C_3^A|^2), \quad (116)$$

$$F_A(q^2) = 4 |\xi_\Lambda(n \cdot p)|^2 \lambda^2 q^2 \text{Re}(C_1^{A*} C_3^A), \quad (117)$$

$$F_L(q^2) = \frac{1}{2} |\xi_\Lambda(n \cdot p)|^2 \lambda (s_+ + s_-) |n(q^2)|^2 (|C_2^A|^2 + |C_4^A|^2), \quad (118)$$

with

$$\begin{aligned} \mathcal{N} &= \frac{1}{128 M_{\Lambda_b}^3 \pi^3}, \quad n(q^2) = \frac{M_{\Lambda_b}^2 - M_\Lambda^2 + q^2 + \lambda}{2 M_{\Lambda_b}}, \\ \lambda &\equiv \sqrt{s_+ s_-} = \sqrt{((M_{\Lambda_b} + m_\Lambda)^2 - q^2)(M_{\Lambda_b} - m_\Lambda)^2 - q^2)}. \end{aligned} \quad (119)$$

Here, the form factor is $\xi_\Lambda(n \cdot p, \mu)$ and the Wilson coefficients C_i^A have been resummed to LL precision as $C_i^A(n \cdot p, \mu)$. The detailed expressions for $C_i^A(n \cdot p, \mu_h)$ can be found in Ref. [24].

For $\Lambda_b \rightarrow \Lambda \gamma$ decay, we have

$$\mathcal{M}(s, s', \lambda) = -\epsilon_\mu^*(q, \lambda) C_\gamma^A(n \cdot p) \xi_\Lambda(q^2 = 0) \bar{u}_\Lambda(p, s') (1 + \gamma_5) \gamma_\perp^\mu u_{\Lambda_b}(v, s). \quad (120)$$

As shown in Ref. [25], we have

$$C_\gamma^A(\mu) = \frac{G_F}{\sqrt{2}} V_{cs}^* V_{cb} \left[C_7^{\text{eff}} + \frac{C_F \alpha_s}{4\pi} (C_8^{\text{eff}} G_8 + \bar{C}_2 G_1(x_c)) \right] (\mu_{\text{QCD}}) \Delta_7 C^A(\mu_{\text{QCD}}, \mu) + \mathcal{O}(\alpha_s^2). \quad (121)$$

In practice, we will take $\mu = \mu_{\text{QCD}} = \mu_h$. The expressions for $G_1(x)$, G_8 and $\Delta_7 C^A$ have been collected in Ref. [25]. The RG equation for C_γ^A is the same as that for the coefficients of the A-type currents in the $\Lambda_b \rightarrow \Lambda \ell^+ \ell^-$ case, so

$$C_\gamma^A(\mu) = \left(\frac{M_{\Lambda_b}}{\mu_h} \right)^{a(\mu_h, \mu)} \exp \left[S(\mu_h, \mu) + \frac{5C_F}{2\beta_0} \ln r_1 \right] C_\gamma^A(\mu_h). \quad (122)$$

Ultimately, we can derive the decay branching ratio as:

$$\begin{aligned} \mathcal{B}(\Lambda_b \rightarrow \Lambda \gamma) &= \frac{\tau_{\Lambda_b}}{16\pi M_{\Lambda_b}} \left(1 - \frac{m_\Lambda^2}{M_{\Lambda_b}^2} \right) \times \frac{1}{2} \sum_{s, s'} \sum_{\lambda=\pm} |\mathcal{M}(s, s', \lambda)|^2 \\ &= \frac{\tau_{\Lambda_b}}{4\pi M_{\Lambda_b}^3} (M_{\Lambda_b}^4 - m_\Lambda^4) |C_\gamma^A(\mu)|^2 |\xi_\Lambda(q^2 = 0)|^2. \end{aligned} \quad (123)$$

³It should be notice that the definition of $\bar{\epsilon}^\mu(\pm)$ in Ref. [58] and $\epsilon^\mu(\pm)$ in Ref. [59] are different with a minus sign, so some results in Eq.(B.3) of Ref. [59] need to change with a minus sign.

References

- [1] LHCb collaboration, *Implications of LHCb measurements and future prospects*, *Eur. Phys. J. C* **73** (2013) 2373 [1208.3355].
- [2] BELLE-II collaboration, *The Belle II Physics Book*, *PTEP* **2019** (2019) 123C01 [1808.10567].
- [3] R.R. Horgan, Z. Liu, S. Meinel and M. Wingate, *Lattice QCD calculation of form factors describing the rare decays $B \rightarrow K^* \ell^+ \ell^-$ and $B_s \rightarrow \phi \ell^+ \ell^-$* , *Phys. Rev. D* **89** (2014) 094501 [1310.3722].
- [4] R.R. Horgan, Z. Liu, S. Meinel and M. Wingate, *Rare B decays using lattice QCD form factors*, *PoS LATTICE2014* (2015) 372 [1501.00367].
- [5] P. Colangelo and A. Khodjamirian, *QCD sum rules, a modern perspective*, hep-ph/0010175.
- [6] A. Khodjamirian, B. Melić and Y.-M. Wang, *A guide to the QCD light-cone sum rules for b-quark decays*, *Eur. Phys. J. ST* **233** (2024) 271 [2311.08700].
- [7] LHCb collaboration, *Angular moments of the decay $\Lambda_b^0 \rightarrow \Lambda \mu^+ \mu^-$ at low hadronic recoil*, *JHEP* **09** (2018) 146 [1808.00264].
- [8] T. Gutsche, M.A. Ivanov, J.G. Korner, V.E. Lyubovitskij and P. Santorelli, *Rare baryon decays $\Lambda_b \rightarrow \Lambda l^+ l^-$ ($l = e, \mu, \tau$) and $\Lambda_b \rightarrow \Lambda \gamma$: differential and total rates, lepton- and hadron-side forward-backward asymmetries*, *Phys. Rev. D* **87** (2013) 074031 [1301.3737].
- [9] P. Böer, T. Feldmann and D. van Dyk, *Angular Analysis of the Decay $\Lambda_b \rightarrow \Lambda(\rightarrow N\pi)\ell^+ \ell^-$* , *JHEP* **01** (2015) 155 [1410.2115].
- [10] LHCb collaboration, *First Observation of the Radiative Decay $\Lambda_b^0 \rightarrow \Lambda \gamma$* , *Phys. Rev. Lett.* **123** (2019) 031801 [1904.06697].
- [11] W. Detmold and S. Meinel, *$\Lambda_b \rightarrow \Lambda \ell^+ \ell^-$ form factors, differential branching fraction, and angular observables from lattice QCD with relativistic b quarks*, *Phys. Rev. D* **93** (2016) 074501 [1602.01399].
- [12] S. Meinel, *Status of next-generation $\Lambda_b \rightarrow p, \Lambda, \Lambda_c$ form-factor calculations*, *PoS LATTICE2023* (2024) 275 [2309.01821].
- [13] Y.-M. Wang, Y.-L. Shen and C.-D. Lu, *$\Lambda(b) \rightarrow p$, Lambda transition form factors from QCD light-cone sum rules*, *Phys. Rev. D* **80** (2009) 074012 [0907.4008].
- [14] T. Feldmann and M.W.Y. Yip, *Form factors for $\Lambda_b \rightarrow \Lambda$ transitions in the soft-collinear effective theory*, *Phys. Rev. D* **85** (2012) 014035 [1111.1844].

- [15] Y.-M. Wang and Y.-L. Shen, *Perturbative Corrections to $\Lambda_b \rightarrow \Lambda$ Form Factors from QCD Light-Cone Sum Rules*, *JHEP* **02** (2016) 179 [1511.09036].
- [16] T. Mannel and Y.-M. Wang, *Heavy-to-light baryonic form factors at large recoil*, *JHEP* **12** (2011) 067 [1111.1849].
- [17] C.W. Bauer, S. Fleming, D. Pirjol and I.W. Stewart, *An Effective field theory for collinear and soft gluons: Heavy to light decays*, *Phys. Rev. D* **63** (2001) 114020 [hep-ph/0011336].
- [18] C.W. Bauer, D. Pirjol and I.W. Stewart, *Soft collinear factorization in effective field theory*, *Phys. Rev. D* **65** (2002) 054022 [hep-ph/0109045].
- [19] M. Beneke, A.P. Chapovsky, M. Diehl and T. Feldmann, *Soft collinear effective theory and heavy to light currents beyond leading power*, *Nucl. Phys. B* **643** (2002) 431 [hep-ph/0206152].
- [20] M. Beneke and T. Feldmann, *Factorization of heavy to light form-factors in soft collinear effective theory*, *Nucl. Phys. B* **685** (2004) 249 [hep-ph/0311335].
- [21] T. Feldmann and N. Gubernari, *Non-factorisable contributions of strong-penguin operators in $\Lambda_b \rightarrow \Lambda \ell^+ \ell^-$ decays*, *JHEP* **03** (2024) 152 [2312.14146].
- [22] R.J. Hill and M. Neubert, *Spectator interactions in soft collinear effective theory*, *Nucl. Phys. B* **657** (2003) 229 [hep-ph/0211018].
- [23] M. Beneke, T. Feldmann and D. Seidel, *Exclusive radiative and electroweak $b \rightarrow d$ and $b \rightarrow s$ penguin decays at NLO*, *Eur. Phys. J. C* **41** (2005) 173 [hep-ph/0412400].
- [24] A. Ali, G. Kramer and G.-h. Zhu, *$B \rightarrow K^+ l^+ l^-$ decay in soft-collinear effective theory*, *Eur. Phys. J. C* **47** (2006) 625 [hep-ph/0601034].
- [25] T. Becher, R.J. Hill and M. Neubert, *Factorization in $B \rightarrow V$ gamma decays*, *Phys. Rev. D* **72** (2005) 094017 [hep-ph/0503263].
- [26] Y.-K. Huang, Y.-L. Shen, C. Wang and Y.-M. Wang, *Next-to-Leading-Order Weak-Annihilation Correction to Rare $B \rightarrow K, \pi \ell^+ \ell^-$ Decays*, *Phys. Rev. Lett.* **134** (2025) 091901 [2403.11258].
- [27] G. Buchalla, A.J. Buras and M.E. Lautenbacher, *Weak decays beyond leading logarithms*, *Rev. Mod. Phys.* **68** (1996) 1125 [hep-ph/9512380].
- [28] M. Beneke, T. Feldmann and D. Seidel, *Systematic approach to exclusive $B \rightarrow V l^+ l^-$, $V \gamma$ decays*, *Nucl. Phys. B* **612** (2001) 25 [hep-ph/0106067].
- [29] M. Beneke and T. Feldmann, *Symmetry breaking corrections to heavy to light B meson form-factors at large recoil*, *Nucl. Phys. B* **592** (2001) 3 [hep-ph/0008255].

- [30] F. De Fazio, T. Feldmann and T. Hurth, *SCET sum rules for $B \rightarrow P$ and $B \rightarrow V$ transition form factors*, *JHEP* **02** (2008) 031 [0711.3999].
- [31] F. De Fazio, T. Feldmann and T. Hurth, *Light-cone sum rules in soft-collinear effective theory*, *Nucl. Phys. B* **733** (2006) 1 [hep-ph/0504088].
- [32] Y.-M. Wang, *Beauty baryon decays: a theoretical overview*, *J. Phys. Conf. Ser.* **556** (2014) 012050.
- [33] M. Beneke and T. Feldmann, *Multipole expanded soft collinear effective theory with nonAbelian gauge symmetry*, *Phys. Lett. B* **553** (2003) 267 [hep-ph/0211358].
- [34] Y.-M. Wang and Y.-L. Shen, *QCD corrections to $B \rightarrow \pi$ form factors from light-cone sum rules*, *Nucl. Phys. B* **898** (2015) 563 [1506.00667].
- [35] M. Beneke, M. Garny, R. Szafron and J. Wang, *Anomalous dimension of subleading-power N -jet operators. Part II*, *JHEP* **11** (2018) 112 [1808.04742].
- [36] J. Gao, C.-D. Lü, Y.-L. Shen, Y.-M. Wang and Y.-B. Wei, *Precision calculations of $B \rightarrow V$ form factors from soft-collinear effective theory sum rules on the light-cone*, *Phys. Rev. D* **101** (2020) 074035 [1907.11092].
- [37] W. Wang, *Factorization of Heavy-to-Light Baryonic Transitions in SCET*, *Phys. Lett. B* **708** (2012) 119 [1112.0237].
- [38] M. Beneke and V.A. Smirnov, *Asymptotic expansion of Feynman integrals near threshold*, *Nucl. Phys. B* **522** (1998) 321 [hep-ph/9711391].
- [39] B. Jantzen, *Foundation and generalization of the expansion by regions*, *JHEP* **12** (2011) 076 [1111.2589].
- [40] V.L. Chernyak, A.A. Ogloblin and I.R. Zhitnitsky, *Wave Functions of Octet Baryons*, *Yad. Fiz.* **48** (1988) 1410.
- [41] V. Braun, R.J. Fries, N. Mahnke and E. Stein, *Higher twist distribution amplitudes of the nucleon in QCD*, *Nucl. Phys. B* **589** (2000) 381 [hep-ph/0007279].
- [42] G. Bell, T. Feldmann, Y.-M. Wang and M.W.Y. Yip, *Light-Cone Distribution Amplitudes for Heavy-Quark Hadrons*, *JHEP* **11** (2013) 191 [1308.6114].
- [43] P. Ball, V.M. Braun and E. Gardi, *Distribution Amplitudes of the Lambda(b) Baryon in QCD*, *Phys. Lett. B* **665** (2008) 197 [0804.2424].
- [44] Y.-L. Liu, C.-Y. Cui and M.-Q. Huang, *Higher order light-cone distribution amplitudes of the Lambda baryon*, *Eur. Phys. J. C* **74** (2014) 3041 [1407.4889].
- [45] S. Groote, J.G. Korner and O.I. Yakovlev, *An Analysis of diagonal and nondiagonal QCD sum rules for heavy baryons at next-to-leading order in alpha-s*, *Phys. Rev. D* **56** (1997) 3943 [hep-ph/9705447].

- [46] Y.-L. Liu and M.-Q. Huang, *Distribution amplitudes of Sigma and Lambda and their electromagnetic form factors*, *Nucl. Phys. A* **821** (2009) 80 [0811.1812].
- [47] R.J. Hill, T. Becher, S.J. Lee and M. Neubert, *Sudakov resummation for subleading SCET currents and heavy-to-light form-factors*, *JHEP* **07** (2004) 081 [hep-ph/0404217].
- [48] S.W. Bosch, R.J. Hill, B.O. Lange and M. Neubert, *Factorization and Sudakov resummation in leptonic radiative B decay*, *Phys. Rev. D* **67** (2003) 094014 [hep-ph/0301123].
- [49] PARTICLE DATA GROUP collaboration, *Review of particle physics*, *Phys. Rev. D* **110** (2024) 030001.
- [50] M. Beneke, *A Quark mass definition adequate for threshold problems*, *Phys. Lett. B* **434** (1998) 115 [hep-ph/9804241].
- [51] Y.-L. Shen, Y.-M. Wang and Y.-B. Wei, *Precision calculations of the double radiative bottom-meson decays in soft-collinear effective theory*, *JHEP* **12** (2020) 169 [2009.02723].
- [52] CDF collaboration, *Precise Measurements of Exclusive $b \rightarrow s\mu^+\mu^-$ Decay Amplitudes Using the Full CDF Data Set*, .
- [53] LHCb collaboration, *Differential branching fraction and angular analysis of $\Lambda_b^0 \rightarrow \Lambda\mu^+\mu^-$ decays*, *JHEP* **06** (2015) 115 [1503.07138].
- [54] LATTICE PARTON collaboration, *Light cone distribution amplitude for the Λ baryon from lattice QCD*, *Phys. Rev. D* **111** (2025) 034510 [2411.12554].
- [55] T. Feldmann and D. Vladimirov, *Radiative tail of the three-particle light-cone distribution amplitudes for the Λ_b baryon in HQET*, 2505.02570.
- [56] Q. Qin, Y.-L. Shen, C. Wang and Y.-M. Wang, *Deciphering the Long-Distance Penguin Contribution to $B^- d,s \rightarrow \gamma\gamma$ Decays*, *Phys. Rev. Lett.* **131** (2023) 091902 [2207.02691].
- [57] Y.-K. Huang, Y. Ji, Y.-L. Shen, C. Wang, Y.-M. Wang and X.-C. Zhao, *Renormalization-Group Evolution for the Three-Particle B-Meson Soft Function*, *Phys. Rev. Lett.* **133** (2024) 171901 [2312.15439].
- [58] D. Das, *Model independent New Physics analysis in $\Lambda_b \rightarrow \Lambda\mu^+\mu^-$ decay*, *Eur. Phys. J. C* **78** (2018) 230 [1802.09404].
- [59] H. Yan, *Angular distribution of the rare decay $\Lambda_b \rightarrow \Lambda(\rightarrow N\pi)\ell^+\ell^-$* , 1911.11568.